

Impact Flashes on the Moon: Cosmic Ray Analysis

Author: **André Muñoz**

Supervisor - Dr. Tony Cook

Department of Mathematics and Physics
Aberystwyth University



This thesis is submitted in partial fulfilment of the
requirements for the Degree of

BACHELOR OF SCIENCE
in
ASTROPHYSICS
with
HONOURS

May 2014

Declaration

STATEMENT 1

The role undertaken by the author within this project was that of experimenter and main researcher, with some assistance from project partner (Mark Staples). All results within this thesis were solely derived by the author.

STATEMENT 2

All contents within this thesis including photographs, figures and tables, were captured and created by the author from scratch unless cited with full reference at the end.

STATEMENT 3

This document was created using L^AT_EX and BIBT_EX. Although great care was taken in its creation, there were bugs in L^AT_EX resulting in some errors. Such include the opening quotation mark appearing as closed, "example". Also, as BIBT_EX entries are automatic, fonts in the reference section are automated. Howbeit, they adhere to Harvard style referencing.

STATEMENT 4

A DVD is included at the rear of all hard copies of this document.

André Muñoz, FRAS
anm47@aber.ac.uk

Aberystwyth University
Department of Mathematics and Physics
Physical Science Building
Aberystwyth
Ceredigion
SY23 3BZ

Abstract

This project analyses the characteristics of cosmic ray particles to distinguish a genuine impact flash on the Moon from false detection. Characteristic features of cosmic ray particles within an image have been identified, however an increase in certainty would aid eliminating false flags, in addition to adding new characteristics to the previously unmentioned or possibly undetected. Magnitude of an impact flash can yield new information about an impact event, and can reveal greater understanding when simulated in a laboratory.

The investigation was carried out by conducting two main experiments. The first occurred in a dark room with the camera lens cap on to capture cosmic ray particles striking the CCD. This took place for seven consecutive days at 10:00 hrs and 22:00 hrs. A total of 14 videos were captured at 50 frames per second for five minutes each. The second experiment was setup to capture a simulated flash at 50 frames per second, with two LED's in the background and foreground for calibration and magnitude calculation. Using a Meade LX200 and Watec 902H CCTV lunar footage was recorded and analysed along with archive data. Three impact flashes were found. 1/3 of the 3 flashes found contained a high uncertainty and may be due to an occulting star. The magnitude for the 'dummy' experiment flash was -10.6 mag. Results from the cosmic rays experiment revealed a characteristic 'L' shape cosmic ray induced pixel. Also a single row/column cosmic ray induced pixel confirmed claims from other investigations, Suggs (2013). In addition, a rare crossed shaped unknown flash was detected during the flash experiment, which is likely to be from a cosmic ray particle colliding with the CCD at a 90 degree angle.

The overall investigation confirms single row/column cosmic ray induced pixel, highlighted previously by other scientists. This project enhances this with the rate at which cosmic ray characteristics occur, and reveal possible new candidates for cosmic ray characteristics to be catalogued.

This page is intentionally left blank

A special dedication to my brothers:

Richard Muñoz (1971-2002)
Lincoln Muñoz (1963-1998)

This page is intentionally left blank

Acknowledgements

It is with immense gratitude that I acknowledge the support and help of my supervisor, Dr. Tony Cook, who was responsible for this project. I would like to thank my tutor, Dr. Balázs Pintér for advising me on certain aspects of the project. Also I wish to thank PhD student, Rachel Cross and Technician, Stephen Fearn for project advice and assistance. In addition, I feel it is only right acknowledge the Department of Mathematics and Physics for giving me the opportunity to work on this project.

I wish to give a special thanks to Petros Tsichlakis, MSc Applied Mathematics (Imperial College London), for advising me on some mathematical points. I would like to acknowledge my aunt, Faith McCully, for the strong support over the years and during this degree. In addition, an acknowledgement to a family friend, Carol Mckenzie for the ongoing encouragement. Finally, a thanks to sister (Donna Muñoz), brother (Norman Muñoz) and close family for the support. Last but not least, a special thanks to my dear mother (Mrs Barbara Muñoz) who witnessed all of my struggles, and father (Mr Michael Muñoz).

This page is intentionally left blank

"...It has been a long journey thus far, with an even longer one ahead of me. However, I believe that nothing is impossible and from my interpretation of quantum mechanics, it is not a matter of possibility but probability"

- André Muñoz

"Dear Andre

You are almost right about everything being possible. But there are some rules. Here is one. Electric charge is conserved. This means that a neutron cannot turn into a proton without an electron being created. But apart from a small number of conservation laws, yes, anything can happen.

Best wishes and good luck on your cosmology journey."

- Leonard Susskind

Contents

1	Introduction	1
2	Literature Review	3
1	Lunar Impact Flash	4
2	Solar System Dynamics	4
3	Observation	4
4	Hypervelocity Impactors	6
5	Different Wavelengths	7
6	Implication on Science	8
7	Problems & False Detection	8
8	Objectives	9
9	Summary	9
3	Procedure	11
1	Preparations	12
2	Equipment & Operations	12
3	Observation	12
4	Laboratory Experiment	14
5	Cosmic Ray Detection	15
6	Data Analysis	15
6.1	Registax	15
6.2	LunarScan	15
6.3	Impact Flash Scanner	15
4	Results	17
1	Observation	18
2	Flash Simulation	18
2.1	Experiment Flash Time Span	20
3	Cosmic Ray Experiment	20
3.1	Background & Cosmic Radiation	20
3.2	Cosmic Ray Samples	23
4	Detected Impact Flashes	23
5	Discussion	27
1	Overall Project Progression	28
2	Cosmic Ray Analysis	28
2.1	Cosmic Ray & Pixel Shapes	28
2.2	The Prominent 'L' Shape	28
2.3	Radial Decrease in Intensity	29
3	Flash Simulation & IFM	29

3.1	Flash Time Considerations	30
4	Detected IFM	31
5	Data Analysis & Software	33
5.1	LunarScan	33
5.2	Registax	33
5.3	Impact Flash Scanner	33
6	Equipment & Hardware	34
7	Background Radiation	34
6	Conclusion	37
	Reference	41
	Glossary	43
	Appendices	45
	Appendix A1: Zoomed Focus	47
	Appendix A2: Specific Software Instructions	48
	Appendix B1: Analysing Archive Data for Impact Flashes	49
	Appendix B2: Experiment Flash Calculation	56
	Appendix C1: Project Plan	58
	Appendix C2: F/6.3 Focal Reducer Derivation	59
	Appendix X1: Risk Assessment	61
	Appendix X2: Impact Flash Scanner C++ Code	62
	Appendix X3: Map of the Moon	71
	Appendix X4: Meteoroid Impact Flash Diagram	73
	Index	75

List of Figures

1.1	Lunar Impact Candidates	2
2.1	Phase Diagram	5
2.2	Lunar Night and Day	7
2.3	Flash and Cosmic Ray Example	8
2.4	Airmass	9
3.1	Dome Navigation	12
3.2	Optical Tube Assembly Diagram	13
3.3	Observational Setup	13
3.4	Flash Simulation Diagram	14
3.5	Simulation Flash Detection	15
4.1	Background Radiation Levels	21
4.2	Detected Daytime Cosmic Rays	22
4.3	Detected Night time Cosmic Rays	22
4.4	Cosmic Ray Samples	23
4.5	Detected Impact Flash 1	23
4.6	Detected Impact Flash 2	24
4.7	Detected Impact Flash 3a	25
4.8	Detected Impact Flash 3b	26
5.1	Cosmic Ray Strike	29
5.2	Event Pixel Comparison	30
5.3	Unknown Flash	31
5.4	Unknown Flash Pixel Diagram	31
5.5	NASA Confirmed IFM	32
5.6	Detected Flash Comparison	32
5.7	Equatorial Wedge	35
5.8	Telescope Mounts	35
1	Zoomed Focus	47
2	Experiment Flash Calculation	56
3	Project Plan	58
4	Field of View	60
5	Lunar Impact Flash 1 Region	71
6	Map of the Moon	72
7	Meteoroid Impact Flash Diagram	73

List of Tables

4.1	Possible Observation	18
1	Analysing Pengdome Archive Data for Impact Flashes 1	50
2	Analysing Pengdome Archive Data for Impact Flashes 2	51
3	Analysing Pengdome Archive Data for Impact Flashes 3	52
4	Analysing Archive Data for Impact Flashes	53
5	Analysing Dr. Cook's Archive Data for Impact Flashes 1	54
6	Analysing Dr. Cook's Archive Data for Impact Flashes 2	55
7	Risk Assessment	61

Nomenclature

m_V	Visual Magnitude
\diamond	Light Emitting Diode (LED)
η	Luminous Efficiency
Ω	Uncertainty
F_{\odot}	Solar Flux-Density
F_{\diamond_1}	Flux of LED Light Source 1
F_{\diamond_2}	Flux of LED Light Source 2
L_{\diamond}	LED Luminosity
V	Volt
v	Velocity
W	Wattage (watt)
A	Ampere (amp)
AVI	Audio Video Interleave
CCD	Charged-Couple Device
deg	Degree
eq	Equation
ESA	European Space Agency
fig	Figure
FPS	Frames Per Second
I	Current
IFM	Impact Flashes on the Moon (plural)
IR	Infra-Red

J Joule
kg Kilogram
L1 Light Source 1 (LED 1)
L2 Light Source 2 (LED 2)
LIF Lunar Impact Flash (singular)
m Meter
mag Magnitude
min Minute
NASA National Aeronautics and Space Administration
nm Nano-Meters $\approx 10^{-9}$ m
OTA Optical Tube Assembly
rad Radian
s Second
TLP Transient Lunar Phenomenon
UV Ultra-Violet
V Visible Wavelength

Chapter 1

Introduction

Impact flashes on the Moon (IFM) are caused by meteoroids from space in addition to being artificially staged, Burchell et al. (2009). Such flashes can be seen without the aid of observational instruments, with fainter impact flashes requiring technological assistance. On average there is approximately one lunar impact flash (LIF) every few hours, Cook (2012b), with nearly 300 impact candidates between 2005 - 2013, Dunbar (2013), fig. 1.1. In general the study of such phenomena gives an understanding of meteoroids and possible threats to planetary or other bodies. An impactor not only yields information about meteoroids tens of grams in size, which are difficult to measure with other techniques, but possible measurements on the energy that is released. Ultimately information about the energy can be determined from finding the magnitude of such impact flashes, along with other known parameters, Suggs (2013).

On 11 September 2013, observations had revealed the brightest LIF ever recorded on the Moon thus far, Madiedo et al. (2014). With a peak brightness of 2.9 ± 0.2 mag in the visual band and lasting 8 s, the impact energy was found along with its mass. Correlation between magnitude and longevity of a LIF has been demonstrated by scientists for sometime, (Bouley et al., 2011). Upon detecting impactors releasing energetic flashes, research has taken place at the Big Bear Solar Observatory in California, USA, to understand the limits to detectability. Research has shown a vari-

ation in brightness over time when regarding the night side of the Moon with reflected light from Earth, (Earth-Shine), Burchell et al. (2007). Detecting a flash and deducing the magnitude is critical in the understanding of incoming meteoroids. Information can be derived from such findings, and partly the main focus of this project.

This report will present some basic but fundamental facts relating the solar system dynamics, and origins of meteoroids which cause IFM. A brief historical account will be given, with examples of previous detected lunar impact flashes to use as a comparative reference for the future. Reviewed literature on observation techniques common to this branch of astronomy will be analysed, along with proposals for improving data. In addition, this report will briefly touch on the science behind impactors at high velocity (Hyper-Velocity Impactors) and detecting IFM in various wavelengths.

Observations were made with a telescope and archive footage scrutinized for IFM. This will be achieved by using visual techniques and the aid of software. Comparisons are made to answer the question of suitability and practicality. Also, the project aims to look into a hypothetical impact flash scenario created in a laboratory, to gain an understanding of how they are detected. From this the project will attempt to calculate the magnitude of a 'dummy' flash and see how information can be

Lunar Impact Candidates

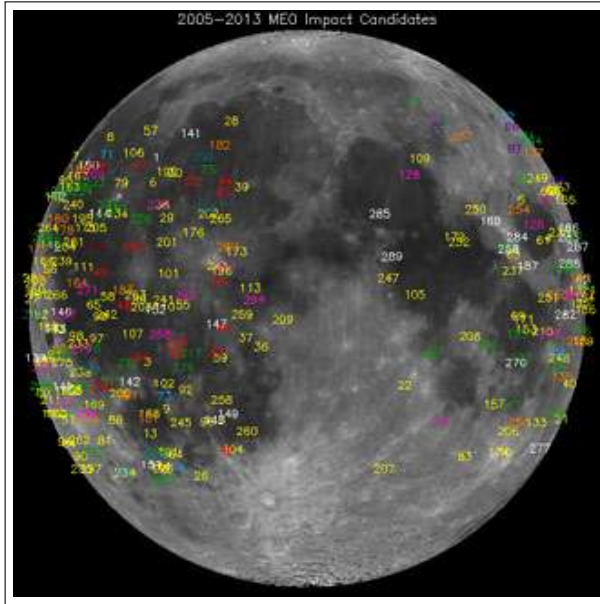


Figure 1.1: The locations of nearly 300 lunar impact candidates between 2005 and 2013, Dunbar (2013). Image quality is low due to lack of similar high resolution images.

extracted and applied to real events.

A requirement for finding IFM are to use two telescopes separated by some distance, Cain (2010), in order to reduce the uncertainty in results. This is common practice throughout institutions who can even collaborate simultaneous observations, Ortiz et al. (2000) and confirm whether a LIF is genuine. However, astronomy is arguably one branch of science that both amateur and professionals can work alongside. As amateur astronomers usually have access to only one telescope, it is critically important to confirm the validity of an impact flash detected with one instrument.

Various obstacles and events can render false flash detections, but the most prominent are cosmic rays. Astronomers have addressed ways of detecting impact flashes from solo observations using techniques to distinguish cosmic rays from genuine impact flashes. Great efforts have been made to scrutinize frames from impact flash footage by analysing the light

distribution over pixels. A uniform pixel light distribution can be indicative of a source that decreases in brightness relatively uniformly in the radial direction. An example is a star or impact flash contrary to cosmic ray strikes that tend to be randomly distributed, Suggs (2013). In addition, Dr. Suggs, (NASA), stated that when a cosmic ray image is pixelated the pixels tend to occupy single rows, columns or pixels. This will be the main focus of this project which analyses cosmic ray images, subject to pixelation in order to help understand their behaviour. Consequently, Dr. Suggs' claim will be analysed from laboratory experiments.

Finally, background radiation experiments are conducted to find the amount of cosmic ray influx during observation. Cosmic ray data captured by a camera's Charged-Couple Device (CCD) are analysed to determine any special features, characteristics which may differ from an impact flash captured in a video frame.

Chapter **2**

Literature Review

Contents

1	Lunar Impact Flash	4
2	Solar System Dynamics	4
3	Observation	4
4	Hypervelocity Impactors	6
5	Different Wavelengths	7
6	Implication on Science	8
7	Problems & False Detection	8
8	Objectives	9
9	Summary	9

1 Lunar Impact Flash

The lunar surface is subject to events which arise from 'hyper-velocity impactors' colliding with the lunar surface. This gives rise to impact flashes, which are a type of Transient Lunar Phenomenon (TLP), meaning change on the Moon, Cudnik (2009). Recorded history has dated the pursuit for IFM back to the early 1940's, Cook (2012a). IFM can be from a natural phenomenon such as meteoroids travelling through space at hyper-velocity, to artificial impact flashes from space craft collisions.

The first successfully recorded LIF occurred for less than 0.02 seconds during the Leonid meteor shower, which was observed in Mexico on 19 November 1999, Ortiz et al. (2000). These were also detected by observers in North America exhibiting magnitudes between 3 - 7 m_V , Dunham et al. (2000). Nearly 300 impact flashes have been catalogued since 2005, Cook (2012a).

2 Solar System Dynamics

There is an intricate relationship between the Sun, Moon and Earth, which governs night and day on Earth and the Moon. Their relative positions are a consequence of lunar phases, which describe the position and illumination of the Moon as seen from Earth, Kutter (2003). When the Moon is between the Earth and Sun, it's phase is denoted as a new Moon. When positioned 180° from new Moon, and Earth is between both Moon and Sun the phase is full, which has 100% illumination, fig. 2.1.

As electromagnetic radiation is emitted from the Sun, it is reflected from both the Earth and Moon's surface back into space. Depending on the relative position of the Moon, a percentage of the lunar surface is visible to observers on Earth. Nevertheless, a fraction is faintly visible due to Earth-shine and separated by a line called the terminator, Zeilik and Gregory (1997a). Commonly, such a

faintly visible part of the lunar surface is called 'night side' and should not be confused with the 'dark side' of the Moon. These dynamics are critical to understanding IFM with good knowledge of their mechanics. Consequently, this can enhance observation technique and chances of detecting an LIF.

It is fundamentally important at this stage to draw emphasis on the relative meaning of meteoroids, meteors and meteorites. Meteoroids are small pieces of solid matter which travel through space, to become meteors upon collision with an atmosphere. If surviving the intense atmospheric friction after impacting the ground, the debris is then called a meteorite, Rothery et al. (2011a). The Earth's orbital path crossing a particular region of orbiting debris, travelling parallel to each other in the same direction gives rise to a meteor shower. As a natural satellite to Earth, the Moon is also prone to bombardment of such objects. Nonetheless, the Moon has a tenuous atmosphere, Sridharan et al. (2010), and suffers from impacts unlike Earth's atmosphere which is dense enough to burn up a meteor in a matter of seconds. It can be argued that due to the atmospheric-like volume the Moon's retained gas is an exosphere. The region of such meteoroids are named after the constellations they appear in relative to the observer. To the contrary, other meteoroids can be random and are termed sporadic. Finally, there are meteoroids which travel from the direction of the Sun, which are thought to be born from Sun-grazing comets and are known as Helion Meteoroids, Cooke et al. (2007).

3 Observation

Observing IFM can be accomplished in numerous ways, with the first taking place in orbit of the Moon from the Lunar Atmosphere and Dust Environment Explorer (LADEE) . In addition, artificial IFM have been produced by ESA, which crashed the SMART-1 space craft on the surface of the Moon in 2006. This was not the sole mission of the spacecraft,

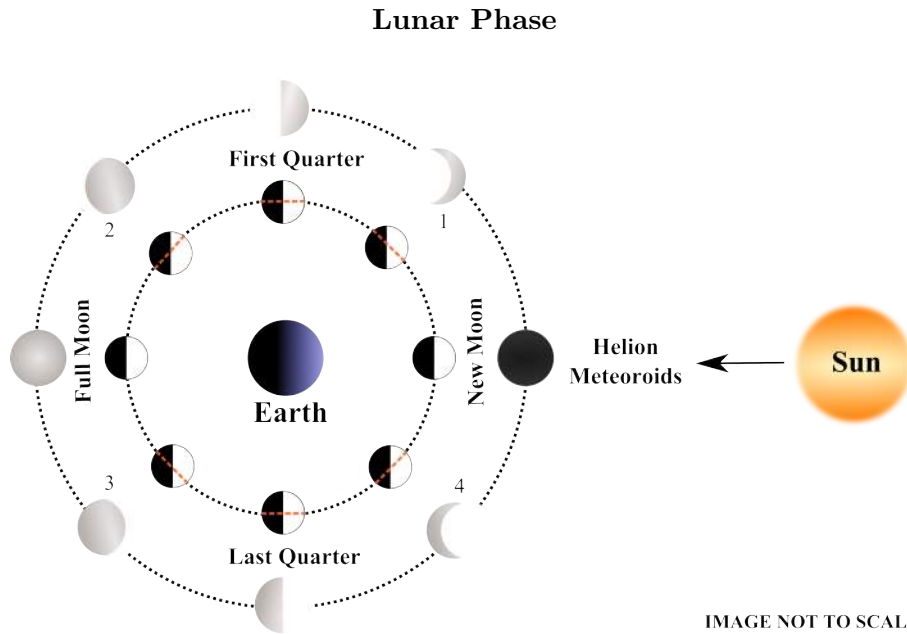


Figure 2.1: Lunar phases denoted by, (1) Waxing Crescent, (2) Waxing Gibbous, (3) Waning Gibbous, (4) Waning Crescent.

Per contra, it's impact played a vital role in understanding the dynamics of an impactor's fraction of kinetic energy being converted into light. Such fraction of kinetic energy being converted into light is termed 'luminous efficiency' (η), which is observed to be dependent on velocity (v). Thus η would be a function of v , Burchell et al. (2009). Recognising this relation, it was found that this brings fourth an understanding that an impact with lower velocity would have a lower fraction of η , than say a hyper-velocity impactor.

The main method of observation concerned in this review is the use of telescopes to detect impact flashes from meteors. Observations of IFM can be achieved with off the shelf telescopes. It can be argued that there are limiting factors that must be considered, such as minimum aperture size, focal length and tracking capabilities. As video frames can be in excess of 5 minutes, smooth continuous footage is needed in order not to miss a potential flash. Two or more telescopes are required for observation to eradicate false detection Cain

(2010); Cook (2012a); Cooke et al. (2007), and can be made sensitive to two different wavebands. More telescopes would decrease the uncertainty in observations and would help achieve increase accuracy in results. Also placing the telescopes further apart can yield an increase in the certainty of IFM. The reason is because parallax may be used to rule out space debris between the Moon and observer.

To observe such faint IFM a $0.25\text{ m} \approx 10\text{ inch}$ telescope would be sufficient enough for observing flashes releasing energies in the visible wavelength (V), and well below $5.0 \times 10^6\text{ J}$, Bellot Rubio et al. (2000). It has also been found that telescopes with a diameter as low as 8 inches can be used to detect IFM. Nonetheless, an argument could be proposed that a decrease in aperture would decrease the detectability at fainter magnitudes. Lower energy impact flashes would have higher probability of detection when viewed near infrared (IR) or the Sodium ($\approx 589\text{ nm}$) part of the electromagnetic spectrum. Thus, increasing the chance of observing such an event, Cooke et al. (2007). Sodium is released by

micro-meteoroid impact vaporisation, Tsembelis et al. (2008) In addition, scattered light from the Moon's day side decreases when observations are near IR, Bellot Rubio et al. (2000), and a flash can be seen to last longer in this waveband. Furthermore, afterglow is possible with detection in both visual (V) and at near IR wavelengths. However, long term afterglow will be better observed in the IR region, Yanagisawa and Kisaichi (2002). This can be due to thermal radiation from ejected hot droplets, which are generated by the impacts, Yanagisawa and Kisaichi (2002).

Impact flashes from hyper-velocity objects involve relatively high velocities therefore, the equipment must not only be sensitive enough, but the detector should contain a high capture frame rate. As most IFM occur for about $1/10^{\text{th}}$ of a second, an imaging detector would be required to capture video frames at $1/50^{\text{th}}$ to $1/60^{\text{th}}$ of a second, Bouley et al. (2011); Cook (2012a); Yanagisawa et al. (2006), which would be suggested for an impactor of 1 kg; travelling at $59 \text{ km}\cdot\text{s}^{-1}$, and observed on Earth as a magnitude 6, Yanagisawa et al. (2006).

When observations are taking place, the telescope's field of view should be sufficiently wide enough so that it covers as much area of the lunar night side as possible, Yanagisawa and Kisaichi (2002), fig. 2.2. This increase in field of view, would boost the chances of detecting a LIF, nevertheless some telescopes are limited in this capacity. A way in which to increase the field of view is to install a focal reducer subsequently, reducing the f-ratio and focal length. In addition enhancing sensitivity of the detector, can be achieved by decreasing integration time. These measures are utilized in Yanagisawa and Kisaichi (2002). A relevant point can be made that the choice of resolution and aspect ratio can increase the chance of detection by a small factor; as this would allow more of the lunar surface to be in the frame with less void at the horizon in the field of view, fig. 2.2.

Once the process of data collection is in mo-

tion, one should be aware that loss of data can occur from dropped frames. The file format for data capture is usually in Audio Video Interleave (AVI) and processed using LunarScan, Gural (2007). This is computer software that contains algorithms to analyse lengthy frames for change in light intensity in a pixel. Therefore possibly ruling out cosmic rays. The software has an advantage of scrutinizing each frame, which can be a tedious job when performed manually.

4 Hypervelocity Impactors

For many years hypervelocity impact flashes have been studied in laboratories using steel spheres impacting steel plates. The experiment can assist understanding by making it possible to predict energy from a light flash, Burchell et al. (2009).

Properties of velocity and mass play a significant and critical role in light being emitted as a flash. The luminous events occur as a result of ejected material being sufficiently heated to such high temperatures, that enough energy is transferred to the material, which then acts as a black body continuum. Consequently, having enough energy to emit its own light. Only a small fraction of kinetic energy from a hypervelocity impact is converted into visible light Burchell et al. (2009).

Bouley et al. (2011) argues that these luminous events are attributed to radiation emitted by small ejecta melt droplets and a cloud composed of gas, (Appendix X4). In the case of a comet, the process involves an expansion of material into a low-density gas cloud after the compression stage. With this, there is an increase in η , which has a greater part of its thermal energy converted into kinetic energy of rapidly cooling vapour. Subsequently, a mere $1/10^{\text{th}}$ to $1/100^{\text{th}}$ of 1% is transformed into radiation, Artem'eva et al. (1999).

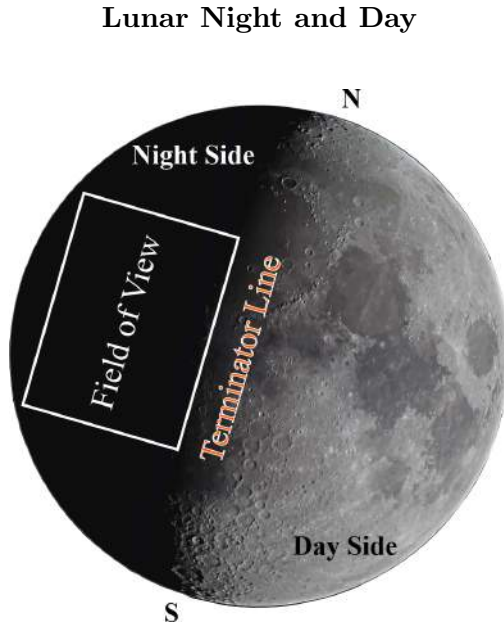


Figure 2.2: The field of view is relatively far away from the terminator line and close to the horizon, in order to gain maximum coverage of the night side, and decrease noise. Also it is important to exclude as much of the day side and terminator to increase the chance of detecting IFM.

5 Different Wavelengths

IFM can be observed through multiple wavebands other than the optical range of 400 - 780 nm, Tipler and Mosca (2008). As the impacts themselves release a vast amount of energy, in the range of 10^6 J, a fraction of the energy is released as light while the remaining is used to form craters. Black-body radiation emitted from these events may allow visible and other wavelengths to be observed, especially beyond the red part of the electromagnetic spectrum. This gives a range of wavelengths to observe, and the ability to calculate the temperature from these flashes. The process is achieved through spectroscopy or using diffraction grating. The brightness of these flashes can be compared to the magnitude of known stars, to determine the temperature, Yanagisawa and Kisaichi (2002). A star is used as collaboration at the beginning of the observation before recording the night side of the Moon. This can sometimes be problematic as recording faint stars may be difficult, due to short exposure times. Bright stars such as Sirius may be an exception.

IFM can be measured in wavelengths lower than the optical range. If the flash is relatively small in the V band, then it would be much shorter as the wavelength decrease in the UV range. Another interesting wavelength to observe is at ≈ 589 nm. It has been suggested that the Moon's exosphere can easily escape its weak gravitational field after a few hours, and is replenished by the meteor impacts, Carbognani and Cremonese (2002). Therefore, observations in the sodium waveband would be a good place to obtain a better understanding of the atmosphere, impact flashes and build temperature models.

Experiments have taken place in laboratories at the University of Kent to simulate the events of an impact flash. The method involves Photomultiplier Tubes (PMT) to determine the average temperature, using iron particles targeting soda-lime glass at velocities of 5 - 20 $\text{km}\cdot\text{s}^{-1}$, Tsemelis et al. (2008).

6 Implication on Science

The occurrence of IFM yield important information on hyper-velocity impacts in general. This may be mass, velocity and chemical composition. Information can be retained about the Moon's exosphere in addition to serving as proof of its low density. An example is the fact that the Moon's tenuous atmosphere serves little as a defence barrier allowing for impacts, as oppose to Earth. The study of IFM can allow for measurements of meteoroids that are several tens of grams in size. Other measuring methods involving such small sizes can be somewhat difficult and challenging. In addition, IFM are critical in understanding the dynamics of the lunar surface and potential hazards from meteors. With future Moon missions that may occur, evaluation of impacts from hyper-velocity objects must be taken into consideration. Such impacts at high velocities, especially with relatively high mass can pose a risk to spacecraft and astronauts on or near the lunar surface. Shrapnel from lower velocity impacts pose more of a risk, as they spread over a large area. In the event of any future manned missions to the Moon, knowledge would be required on the risk of impactors in an environment, which has nearly no atmosphere for protection. Careful consideration must be made as health risks increase on manned missions through the commutation of hyper-velocity impact ejecta forming clingy and sharp agglutinate, Cain (2010).

7 Problems & False Detection

As lunar phase increase beyond 60 % observations are affected due to scattering within the Earth's atmosphere, Cook (2012a). Some observers may draw a limit between 10 % and 50%, Cooke et al. (2007). Nonetheless, it can be suggested that it depends on certain parameters, including sensitivity of equipment, atmospheric conditions, the Moon's declination in the sky and other attributes. With a typical surface illumination between 20-30 % of the lunar surface, the Moon's 'night side'

has a brightness in the order of $m_V = 12 \text{ mag arcsec}^{-2}$, and increases in magnitude with increasing lunar phase, (Bellot Rubio et al., 2000).

There are objects and situations that can produce a flash, glint of light, or scintillation which may yield false readings. These range from objects in deep space (i.e star light), space debris, cosmic rays and TLPs. An example is Sun light which can be reflected from artificial satellites, leading to false impact detection. Methods have been implemented to combat this problem by cataloguing the position of space debris and satellites at times of impact flashes, Yanagisawa and Kisaichi (2002).

Flash and Cosmic Ray Example



Figure 2.3: A likely cosmic ray image superimposed on an artificial flash, extract from an experiment to demonstrate similarities. The image has been cropped and mono-chromed to simulate a real world environment, with the brightness slightly enhanced. The likely captured cosmic ray is on the bottom right of the image with the flash in the upper left.

Natural background radiation is present on Earth and is everywhere. Around 5 % is from space, EPA (2013) in the form of cosmic rays, Poje et al. (2011). These high energy particles can result in problems detecting IFM as they appear similar to impact flashes in images, fig. 2.3. It is therefore paramount to distinguish the two and is a main focus in this project. Due to the nature of relatively faint impact flashes on the lunar night side in contrast to a highly luminous day side, it can be challenging

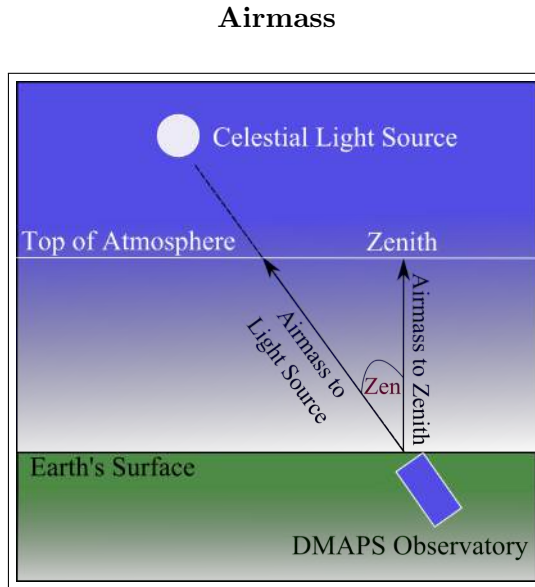


Figure 2.4: A demonstration of how airmass increases with decreasing declination above the horizon. Subsequently, the light from celestial sources are attenuated.

to decipher radiation emitted from an impact. Such a dilemma would lead to the concern of signal-to-noise ratio, where the noise can be attributed to light scattered from the luminous day side of the Moon and even Earth shine. Precautions may be taken to limit this problem, by observing during phases between 10-50 %. In addition the relative position of the Moon in the sky exhibits a problem when close to the horizon, where the atmosphere is thicker between the Moon and observer, fig. 2.4.

8 Objectives

Hundreds of LIF have been detected since first captured from the Leonid's meteor shower. The goals are to increase understanding of meteor showers, and hyper-velocity impactors, which cannot be achieved through Earth based experiments. More observations and detection of impact flashes through multiple wavebands can yield a more thorough understanding of energy released. From this, vital information can be deduced through the study of this energy in different wavebands and build a temperature profile.

9 Summary

IFM occur mainly due to hyper-velocity impacts from meteoroids, nonetheless can be artificial in the form of a unmanned spacecraft, Burchell et al. (2009). Many unknown facts can be revealed from such flashes however, the longevity are relatively short lived, lasting in the region of 0.1 seconds.

As there are many cases which can lead to false detection such as scintillation, space debris, cosmic rays and noise, two telescopes should be used. This is because in the case of a cosmic ray being detected in one detector the probability of being detected in another is very low. Often, in the case of amateur astronomy access to two telescopes is unlikely. The process of eradicating suspect cosmic rays become more challenging, with the need to device greater methods in reducing uncertainties in impact flash detection. Finally, with regards to the implications on science IFM can be used to understand the physics and dynamics of the solar system.

Chapter **3**

Procedure

Contents

1	Preparations	12
2	Equipment & Operations	12
3	Observation	12
4	Laboratory Experiment	14
5	Cosmic Ray Detection	15
6	Data Analysis	15
6.1	Registax	15
6.2	LunarScan	15
6.3	Impact Flash Scanner	15

1 Preparations

The first thing in preparing for observing the Moon was to investigate the weather forecast on the day concerned. Authoritative sources were consulted for reliability, such as the Met Office, British Broadcasting Corporation in addition to the weather station at the Department of Mathematics and Physics (DMAPS).

With clear sky forecasts, last minute checks were in place ensuring no overcast or strong winds. It was critical to make certain that wind speeds were below 25 mph and gusts remained below 30 mph. Furthermore images from observations can become somewhat unstable, however this is dependant on the size of the telescope and pier which it is mounted on. A time stamp of IFM is imperative when verifying an event with other observers, so an atomic clock was used via the internet, Word-TimeSavers (1998).

2 Equipment & Operations

Using remote desktop software, automatic star alignment was completed for the purpose of tracking and using the 'go-to' feature. When tracking the Moon, final checks were in place to establish the tracking rate was set at 'lunar-rate'. Manual operations were sometimes performed in which an auto-alignment was not required. It is important to keep a close eye on the telescopes motion (depending on set-up) as it approaches the meridian, fig. 3.1. When the Optical Tube Assembly's (OTA) rear is perpendicular to the meridian, tension may become high in cables causing damage. In the case of a telescope mounted on a German equatorial mount (GE), crossing the meridian may result in a necessary flip on its axis leading to subsequent damage to equipment. With successful tracking, focusing was set to obtain clarity within the image/video using robo-focus.

The equipment used for observation at DMAPS was within the recommended specifi-

cation advised by astronomers, Cudnik (2013). A set-up diagram along with the equipment used can be seen in fig. 3.2 and fig. 3.3.

Dome Navigation

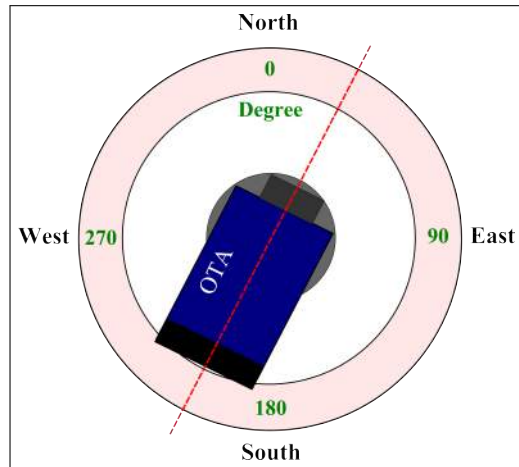


Figure 3.1: Observatory navigation with the OTA's front pointing towards south west. This is the parking position, with the dotted line representing the meridian.

3 Observation

The Moon's view through the CCTV was positioned to include only the night side, (see fig. 2.2). Calculations were performed to determine the field of view (θ) in order to understand how much of the lunar surface can be captured in one frame. The field of view depends on focal length, fig. 3.2, of an OTA and field stop of the eyepiece or CCD chip-size. This is important as the field of view can increase or decrease the chance of observing an IFM. Using a Watec 902H CCTV with a chip-size (d_{CCD}) of 12.9 mm, θ was calculated using the Pythagorean theorem, eq. 3.1, where w = width and h = height of the chip. The field of view of 0.3° was determined from eq. 3.4, Norton (2004a).

Optical Tube Assembly Diagram

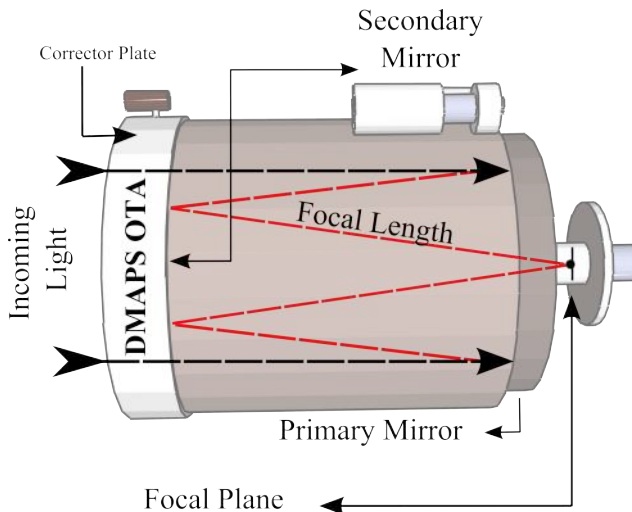


Figure 3.2: An internal view of the OTA in fig. 3.3. Incoming light rays enter the OTA's front which is reflected off the primary mirror onto the secondary mirror. The light is converged to a focal point (focal plane) at the rear.

Observational Setup

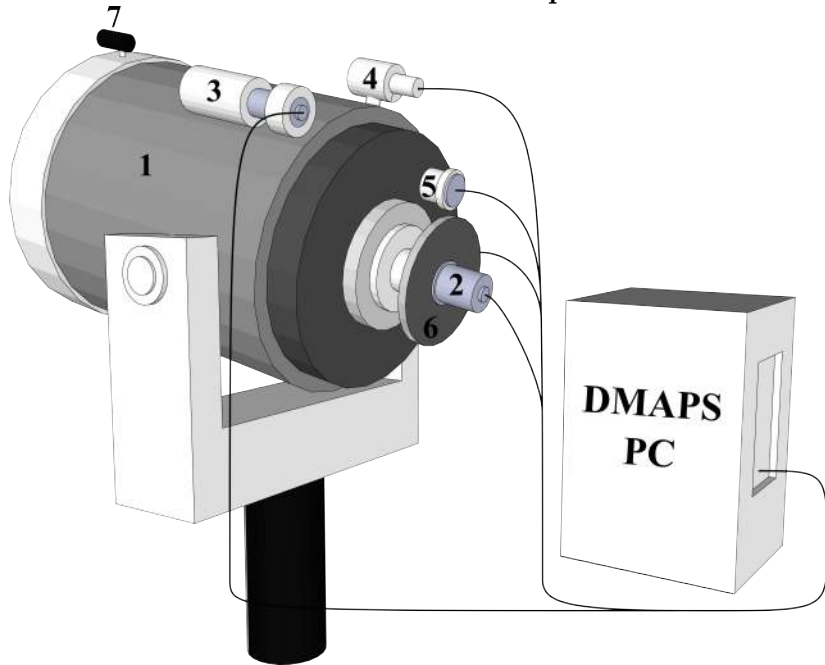


Figure 3.3: The observational setup at Aberystwyth University. (1) Meade LX200 10 inch OTA on a alt-azimuth mount, which sits on a pier. (2) Watec 902H CCD camera. (3) LPI camera attached to the OTA's finder/guide scope. (4) Narrow angle CCTV. (5) Robo-Focus for automatic and remote focusing. (6) Filter wheel and (7) Wide field of view CCTV.

Flash Simulation Diagram

$$d_{CCD} = \sqrt{w^2 + h^2} \quad (3.1)$$

$$= \sqrt{(9.8 \text{ mm})^2 + (8.4 \text{ mm})^2} \quad (3.2)$$

$$= [12.9 \text{ mm}] \quad (3.3)$$

Once d_{CCD} was found this was used to determine θ .

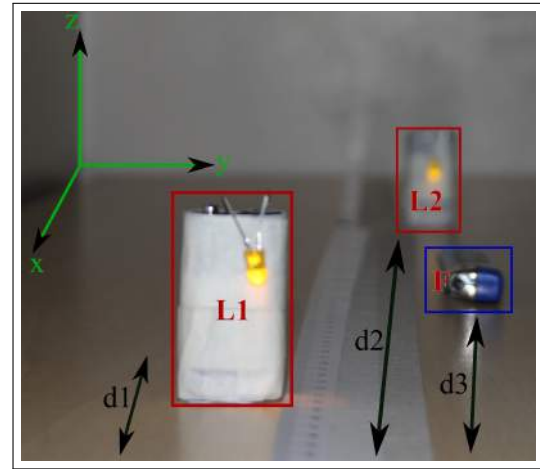


Figure 3.4: Two lights sources are placed at different distances along the x-axis with the same power (L1 and L2). A piezo igniter replicating an impact flash is also placed at some distance (d_3) along the x-axis, between both light source.

$$\theta = \frac{d_{CCD}}{f_o} \quad (3.4)$$

$$= \frac{12.9 \text{ mm}}{2.5 \times 10^3 \text{ mm}} \quad (3.5)$$

$$= 5.2 \times 10^{-3} \text{ rad} \quad (3.6)$$

$$= 5.2 \times 10^{-3} \text{ rad} \left(\frac{180}{\pi} \right) \text{ deg} \cdot \text{rad}^{-1} \quad (3.7)$$

$$= 0.295 \text{ deg} \quad (3.8)$$

$$= [0.3^\circ \text{ to } 1 \text{ s.f.}] \quad (3.9)$$

With the relevant part of the lunar surface in field of view, focusing was achieved using robo-focus. This can be a difficult procedure so focusing on a crater with increased zoom was performed to gain maximum clarity. Once satisfied a relatively sharp focus was obtained at normal magnification, Appendix A1. In addition large values in the hundreds were used to begin the focusing process then smaller values in the tens for fine tuning.

4 Laboratory Experiment

A tape measure was adhered to a table and the camera's CCD (Canon EOS 60D) placed

at zero meters along a fictitious x-axis, fig. 3.4. The light source L1 was positioned at a distance (d_1) of 0.50 meters (m) from the CCD, and the second light source L2 placed at double the distance (d_2) of 1 meter. Subsequently 1/4 the photons would reach the CCD as governed by the inverse square law. Both light sources were representations of an occulting star in the video frame. Using a Piezo igniter to create a single spark placed at distance (d_3) of 0.7 m, this would replicate an IFM. Both light source were powered by 2×AA batteries at 1.5 V each.

A 'Bias-frame' was captured with 1/8000th s exposure and used as reference in each video frame. Using Virtual Dub, Virtual (2005) the AVI was converted to a Bitmap file (BMP). One 'Dark-frame' was captured at the minimum ISO setting of 100 to reduce noise with an exposure time of 60 s. Such long exposure time can only be achieved by using the 'Bulb' setting on a Canon EOS 60D.

A video was recorded with a resolution of 1280×720 at 50 frames per second (FPS). The recording length was 60.36 s, with the 'dummy flash'

occurring at 30 s, fig. 3.5.

ysis.

Simulation Flash Detection



Figure 3.5: The experimental flash detected by Registax and circled yellow represents an IFM, with the two orange light sources as occulting stars.

Some files were filmed with a Canon 60D containing a MOV file output. The MOV files were converted into AVI's using MPEG Streamclip, Cinque (2005) to be imported into Registax 5, Berrevoets (2011). On various occasions some natively captured AVI files encountered difficulties importing into Registax 5 due to codec problems. These files were opened in Virtual Dub, Virtual (2005) and exported as an AVI file.

The AVI file was imported into Registax 5 and a value of 4.0 was selected for sigma. The detection region was resized for processing so that there was maximum image coverage, and any flash detected with a frame would be circled yellow, fig. 3.5.

6.2 LunarScan

LunarScan Gural (2007) was also used for data analysis, with the first process ensuring that all AVI files were placed in the sub folder within the programs folder. Within the program initial steps were made to confirm that the AVI worked. The scanning area was selected for each video and scanned for impact flashes. Specific instructions for using LunarScan are described in Appendix A2.

6.3 Impact Flash Scanner

Impact Flash Scanner (IFS), Cook (2004) first had to be compiled and was executed using MinGW, Colin (2005). The software is compatible with resolutions 720×480 , 540×480 NTSC and 768×576 PAL, thus some AVI's were resized in Virtual Dub.

5 Cosmic Ray Detection

Background radiation counts were recorded for $52^{\circ} 24' 55.8864''$ N lat and $4^{\circ} 3' 47.0376''$ W long, using a Radex 1503 Geiger counter. Subsequently, an experiment was conducted to detect cosmic rays using a Canon EOS 60D. The camera was placed in a dark room away from any other electronic device and possible radiation source. With the CCD facing north and lens cap on, 1 minute videos were recorded. Each video was captured at 50 FPS along with bias-frames at $1/8000^{\text{th}}$ exposure time at the beginning. This was repeated once in the morning, and 12 hours later in the evening for 7 consecutive days. The data was subsequently analysed in Registax for signs of cosmic rays.

6 Data Analysis

6.1 Registax

All files were recorded or converted in to AVI's, as used by most software for impact flash anal-

Chapter **4**

Results

Contents

1	Observation	18
2	Flash Simulation	18
2.1	Experiment Flash Time Span	20
3	Cosmic Ray Experiment	20
3.1	Background & Cosmic Radiation	20
3.2	Cosmic Ray Samples	23
4	Detected Impact Flashes	23

1 Observation

Observation opportunities throughout the project were recorded based on the amount of relevant portions of the Moon in view. The number of permitted observation nights result from the Moon's position approximately 15 - 45° above the horizon, Gates (2004). This is also based on a 10 - 60 % lunar phase two hours after astronomical twilight, Table 4.1.

Possible Observation

Month (A)	Dates (B)	Obs (C)	Weather (D)
Oct 2013	11,12	2	Overcast
Nov 2013	10	1	Overcast
Dec 2013	9	1	Overcast
Jan 2014	23	1	Overcast
Feb 2014	5,6	2	Overcast
Mar 2014	5,6,7,8	4	Haze

Table 4.1: (A) is the month, (B) dates when relevant observations could take place, (C) number of observations permitted for the month, (D) is the weather conditions for all nights within a specific month.

2 Flash Simulation

An experiment was conducted to replicate an impact flash using LED's, along with a spark from a Piezo igniter. The LED's luminosity¹ (L_{\diamond}) with its uncertainty was calculated, eq. 4.3., using eq. 4.1, Beiser (1995); where (I) is the current and (V) is the voltage. Using manufacturer's specification for the LED an error (Ω_I) of $\pm 0.001 A$ was determined for

¹The LED's illumination is not constant in all directions. In addition the luminosity calculated is not completely accurate as there are other considerations. Thus, the luminosity's uncertainty is for demonstration and showing scientific practice. Consequently, uncertainties in equations which are derived from L_{\diamond} , (magnitude and flux), will not be calculated as they will not bear any relevance. Please note, this is for theoretical illustration only.

the current. For the battery a volt meter was used to find the error (Ω_V) of $\pm 0.001 V$.

$$L_{\diamond} = IV \quad (4.1)$$

$$= 0.01 A \cdot (3.0 V) \quad (4.2)$$

$$= (0.030 \pm 0.003) W \quad (4.3)$$

The uncertainty for the LED (Ω_{\diamond}) was derived from eq. 4.4, Hughes (2009), where watts $W = VA = \text{kg} \cdot \text{m}^2 \cdot \text{s}^{-3} \cdot A^2 \cdot \mathcal{K}$.

$$|\Omega_f| = \sqrt{\left(\frac{\partial f}{\partial a}\right)^2 \Omega_a^2 + \left(\frac{\partial f}{\partial b}\right)^2 \Omega_b^2} \quad (4.4)$$

$$|\Omega_{L_{\diamond}}| = \sqrt{\left(\frac{\partial L_{\diamond}}{\partial I}\right)^2 \Omega_I^2 + \left(\frac{\partial L_{\diamond}}{\partial V}\right)^2 \Omega_V^2} \quad (4.5)$$

$$= \sqrt{\left(\frac{\partial IV}{\partial I}\right)^2 \Omega_I^2 + \left(\frac{\partial IV}{\partial V}\right)^2 \Omega_V^2} \quad (4.6)$$

$$= \sqrt{(V)^2 \Omega_I^2 + (I)^2 \Omega_V^2} \quad (4.7)$$

$$= \sqrt{9 \times 10^{-6} W^2 + 1 \times 10^{-10} W^2} \quad (4.8)$$

$$= \sqrt{9 \times 10^{-6}} \sqrt{W^2} \quad (4.9)$$

$$= [0.003 \text{ to } 1 \text{ s.f.}] \quad (4.10)$$

Once L_{\diamond} was calculated, the brightness for each LED was found by using the brightness (Flux Density F) luminosity equation, Roos (2003), eg. 4.11, where $F_{\diamond 1}$ = flux of LED light source 1, and d = distance from camera CCD.

$$F_{\diamond 1} = \frac{L_{\diamond}}{4\pi d^2} \quad (4.11)$$

$$= \frac{0.03 W}{4\pi(0.50 m)^2} \quad (4.12)$$

$$= 9.5 \times 10^{-3} W \cdot m^{-2} \quad (4.13)$$

$$= [0.0095 W \cdot m^{-2} \text{ to 2 s.f.}] \quad (4.14)$$

The same calculations were performed for the second light source, $F_{\diamond 2}$ = flux of LED light source 2, eq. 4.15.

$$F_{\diamond 2} = \frac{L_{\diamond}}{4\pi d^2} \quad (4.15)$$

$$= \frac{0.03 W}{4\pi(1 m)^2} \quad (4.16)$$

$$= [0.0024 W \cdot m^{-2} \text{ to 2 s.f.}] \quad (4.17)$$

Once the flux-density was calculated for each light source within the experiment, L1 and L2, (fig. 3.4), information about the flash was determined. Next the solar flux-density (F_{\odot}) was found, eq. 4.18, where, $L = 3.84 \times 10^{26} W$, and the Earth-Sun distance is $d = 1.50 \times 10^{11} m$. In addition, the flash flux-density was calculated, (F_*), eq. 4.20, where L was estimated to be the same as the LED. (See Appendix B2 for true calculation).

$$F_{\odot} = \frac{3.84 \times 10^{26} W}{4\pi(1.50 \times 10^{11} m)^2} \quad (4.18)$$

$$= [1358 W \cdot m^{-2} \text{ to 4 s.f.}] \quad (4.19)$$

$$F_* = \frac{0.003 W}{4\pi(0.7 m)^2} \quad (4.20)$$

$$= [0.00049 W \cdot m^{-2} \text{ to 2 s.f.}] \quad (4.21)$$

Using equation 4.22, the relative magnitude (m_{R_1}) of L1 was found, (eq. 4.23) where the Sun's visual magnitude is $m_{V_{\odot}} = -26.75$, Zeilik and Gregory (1997b). Additionally, the relative magnitude (m_{R_2}) of L2 was deduced. (eq. 4.26).

$$m_{V_{\odot}} - m_{R_1} = -2.5 \log \left(\frac{F_{\odot}}{F_1} \right) \quad (4.22)$$

$$m_{R_1} = m_{V_{\odot}} + 2.5 \log \left(\frac{F_{\odot}}{F_1} \right) \quad (4.23)$$

$$= -26.75 + 2.5 \log \left(\frac{1358}{0.0095} \right) \quad (4.24)$$

$$= [-13.9 \text{ to 3 s.f.}] \quad (4.25)$$

$$m_{R_2} = m_{V_{\odot}} + 2.5 \log \left(\frac{F_{\odot}}{F_2} \right) \quad (4.26)$$

$$= -26.75 + 2.5 \log \left(\frac{1358}{0.0024} \right) \quad (4.27)$$

$$= [-12.4 \text{ to 3 s.f.}] \quad (4.28)$$

Using similar procedures the experiment flash's relative magnitude (m_{R_*}) was found, eq. 4.29 by using m_{R_1} and $F_{\diamond 1}$.

$$m_{R*} = m_1 + 2.5 \log \left(\frac{F_1}{F_*} \right) \quad (4.29)$$

$$= -13.9 + 2.5 \log \left(\frac{0.0095}{0.00049} \right) \quad (4.30)$$

$$= [-10.7 \text{ to } 3 \text{ s.f.}] \quad (4.31)$$

$$t_i = \frac{VD_L}{FR} \quad (4.37)$$

$$= \frac{60.36 \text{ s}}{3018 \text{ fr}} \quad (4.38)$$

$$= \frac{1}{50} \frac{\text{s}}{\text{fr}} \quad (4.39)$$

$$= [2.0 \times 10^{-2} \text{ s} \cdot \text{fr}^{-1}] \quad (4.40)$$

2.1 Experiment Flash Time Span

The experiment flash was brief and could have gone undetected by the human eye upon blinking. A video capture length of 60.36 s was taken at a frame rate of 50 FPS = 50 fr · s⁻¹. The total number of captured frames was calculated, eq. 4.32, where FR = number of frames (units (fr)), VD_L = video length (units in seconds (s)) and FPS = Frames Per Second.

$$FR = FPS \cdot (VD_L) \quad (4.32)$$

$$= 50 \text{ fr} \cdot s^{-1} (60.36 \text{ s}) \quad (4.33)$$

$$= [3018 \text{ fr}] \quad (4.34)$$

The flash occurred once in 3018 frames and from equation 4.40, it can be concluded that the experiment flash time span was approximately equal to t_i. 2.0 × 10⁻² s. Namely, the flash from the experiment with an estimated error lasted (0.02 ± 0.01)s in the V band. If the flash was to occur over a number of frames then the total flash time would be the sum of t_i or exposure time (EV).² From this a general formula was derived to find a flash's time span, eq. 4.41.

$$EV \simeq \sum_{\mu=1}^n (t_i)_\mu \quad (4.41)$$

$$(\mu = 1, 2, 3, \dots, n)$$

From the number of frames and video length, calculations were performed to find the integration time of each frame (t_i), eq. 4.35. Findings have revealed that (t_i) is equal to the reciprocal of FPS with units in seconds per frame (s · fr⁻¹).

$$\frac{1}{FR} = \frac{1}{FPS \cdot VD_L} \quad (4.35)$$

$$\frac{VD_L}{FR} = \frac{1}{FPS} = t_i \quad (4.36)$$

3 Cosmic Ray Experiment

3.1 Background & Cosmic Radiation

Using a digital Geiger counter the background radiation levels were record. Recorded in cycles of 40 s over 52 cycles, the whole background radiation experiment lasted 2080 s, around 34 minutes. Recorded in Sieverts (Sv) and averaged over an hour the dimensions of each count was in micro Sieverts per hour (μSvh⁻¹), fig. 4.1.

²Exposure may take on a slightly altered meaning from a photographers definition.

Background Radiation Levels

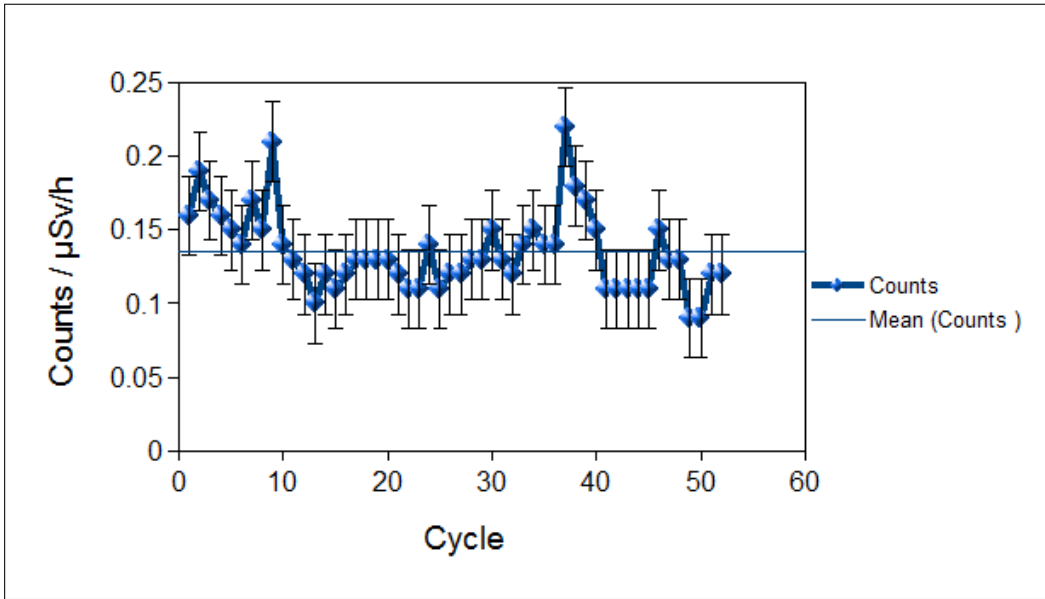


Figure 4.1: Background radiation levels recorded using a Radex 1503 Geiger counter. The measurements are in counts as a function of cycles, where one cycle is 40 seconds. The mean count is calculated and displayed as a horizontal light blue line with a value $\tilde{x} = 0.14 \mu\text{Sv} \cdot \text{h}^{-1}$. The Error bars are standard deviation.

Data from a series of cosmic ray experiments over seven days was documented, fig. 4.2, fig. 4.3. One in the day and another set at night. The number of detected cosmic rays were recorded each day and night with the mean (\tilde{x}) calculated, eq. 4.43 and eq. 4.44, from the last part of equation 4.42. N is the number of samples.

Furthermore, the standard deviation (σ) was found from the initial part of equation 4.42 where N is the number of samples and x_i is the sample. Finally values for standard error of the mean (SEM) were derived, eq. 4.47 with a value of $SEM_{day} = 1.05$ for cosmic rays detected in the day and $SEM_{night} = 1.44$ detected at night, eq. 4.48.

$$\tilde{x} = \frac{1}{N} \sum_{i=1}^N x_i$$

$$(i = x_1 + x_2 + \dots + x_N)$$

$$\tilde{x}_{day} = 5.6 \quad (4.43)$$

$$\tilde{x}_{night} = 5.1 \quad (4.44)$$

$$\tilde{x}_{gen} = 5 \quad (4.45)$$

$$SEM = \frac{\sigma}{\sqrt{N}} \quad (4.46)$$

$$SEM_{day} = 1.05 \quad (4.47)$$

$$SEM_{night} = 1.44 \quad (4.48)$$

$$\sigma = \sqrt{\frac{1}{N} \sum_{i=1}^N (x_i - \tilde{x})^2} \quad (4.42)$$

where,

Detected Daytime Cosmic Rays

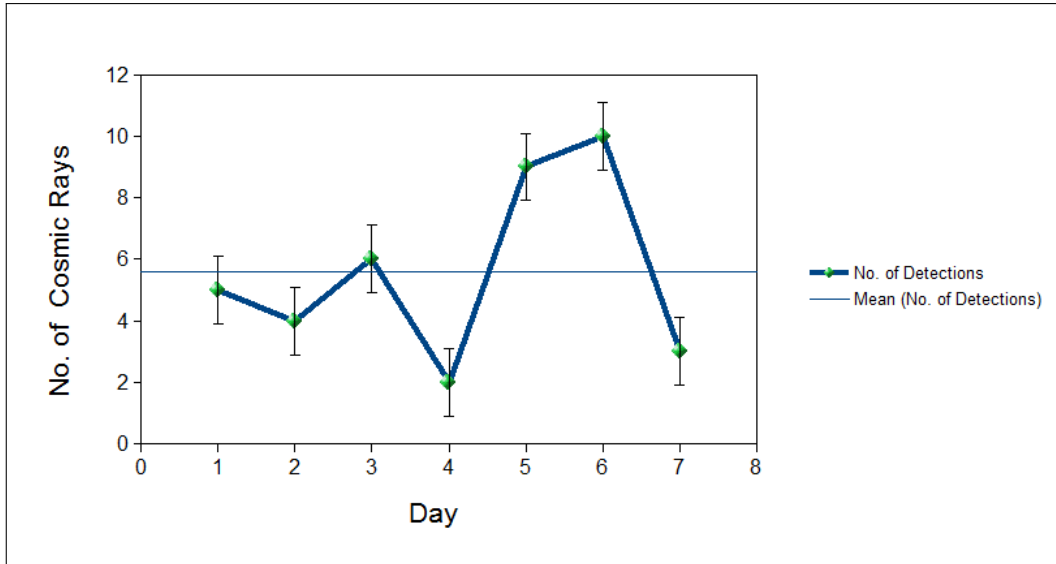


Figure 4.2: A plot of detected cosmic rays as a function of date (Day). The horizontal light blue line is the mean number of detections, (eq. 4.43). Error bars represent error of the mean, (eq. 4.46).

Detected Night time Cosmic Rays

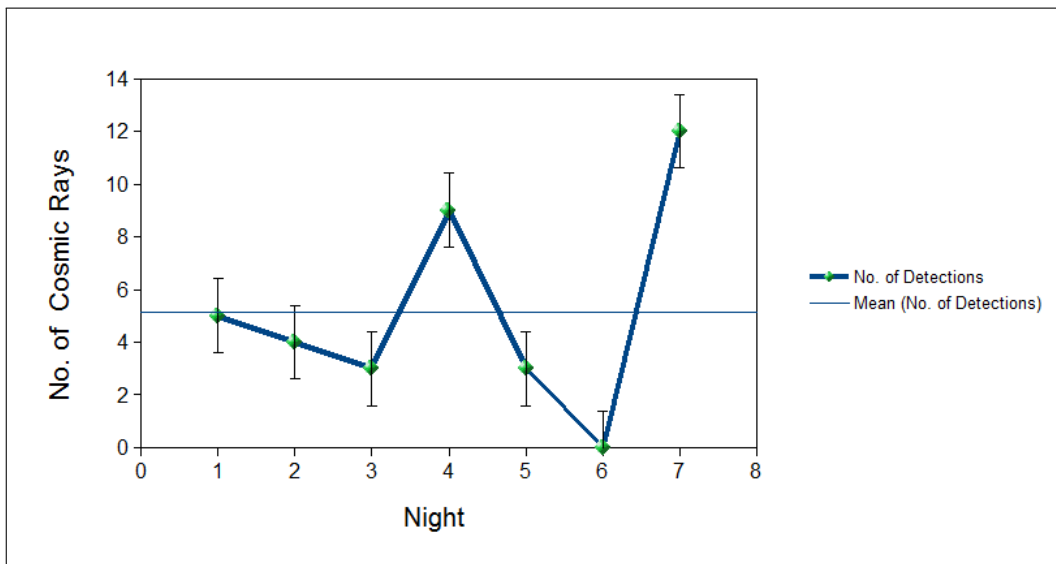


Figure 4.3: A plot of detected cosmic rays as a function of date (Night). The horizontal light blue line is the mean number of detections, (eq. 4.44). Error bars represent error of the mean, (eq. 4.47).

3.2 Cosmic Ray Samples

The cosmic ray experiment detected an overall average (\tilde{x}_{gen}) of 5 cosmic rays per min. Six of the most prominent samples were extracted from data files for analysis and comparison, fig. 4.4.



Figure 4.4: Cosmic ray samples extracted from the experiment. Each sample has its magnification increased along with enhanced brightness, in order for features to be distinguished. A sample has been named according to the date of capture, ending with the letters d = day and n = night.

4 Detected Impact Flashes

21.32 hours of archive data was analysed using various methods such as LunarScan, Impact Flash Scanner and Virtual Dub. Each file was logged, scrutinized and categorized according to the quality of footage. Out of the 21.32 hours three flashes were detected within the

footage, Appendix B1.

Detected Impact Flash 1

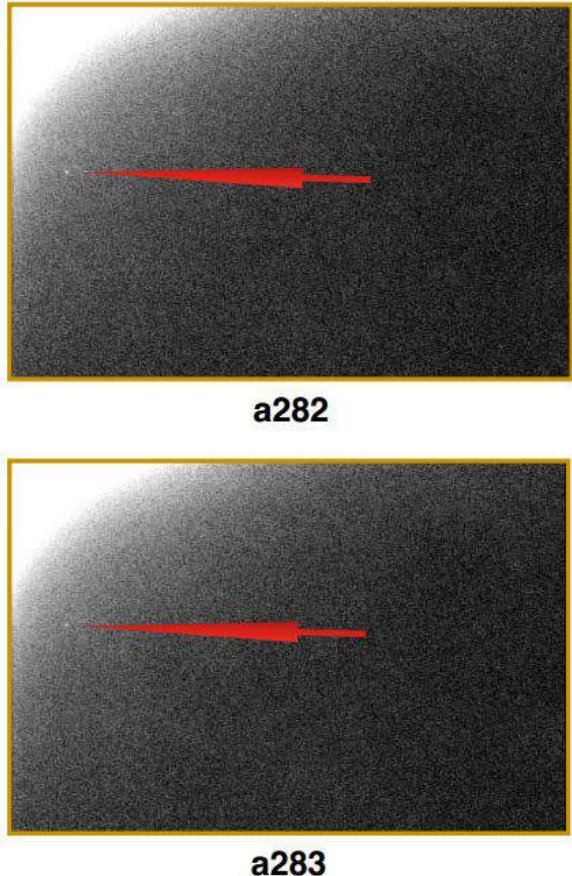


Figure 4.5: LIF captured 18 November 2001, 23:19:15 UTC near Tranquillitatis/Serenitatis lasting 0.065 s, eq.4.50. Flash occurring in frames a282 and a283. Image extracted from footage courtesy of Cook (2014)

On 18 November 2001, 23:19:15 UTC near Tranquillitatis/Serenitatis region an LIF was detected in the V band and found using virtual dub. The event took place near the terminator line and lasted a period over two image frames. Initially, the flash appear at its peak in frame (a282) and decreases in brightness in frame (a283), fig. 4.5. On 19 November 2001, 00:18:58 UTC another LIF was detected in the V band and found using virtual dub. It occurred over a period of three frames starting at frame (a1830), peaking in frame (a1831) and disappears after frame (a1832), fig. 4.6. The

Detected Impact Flash 2

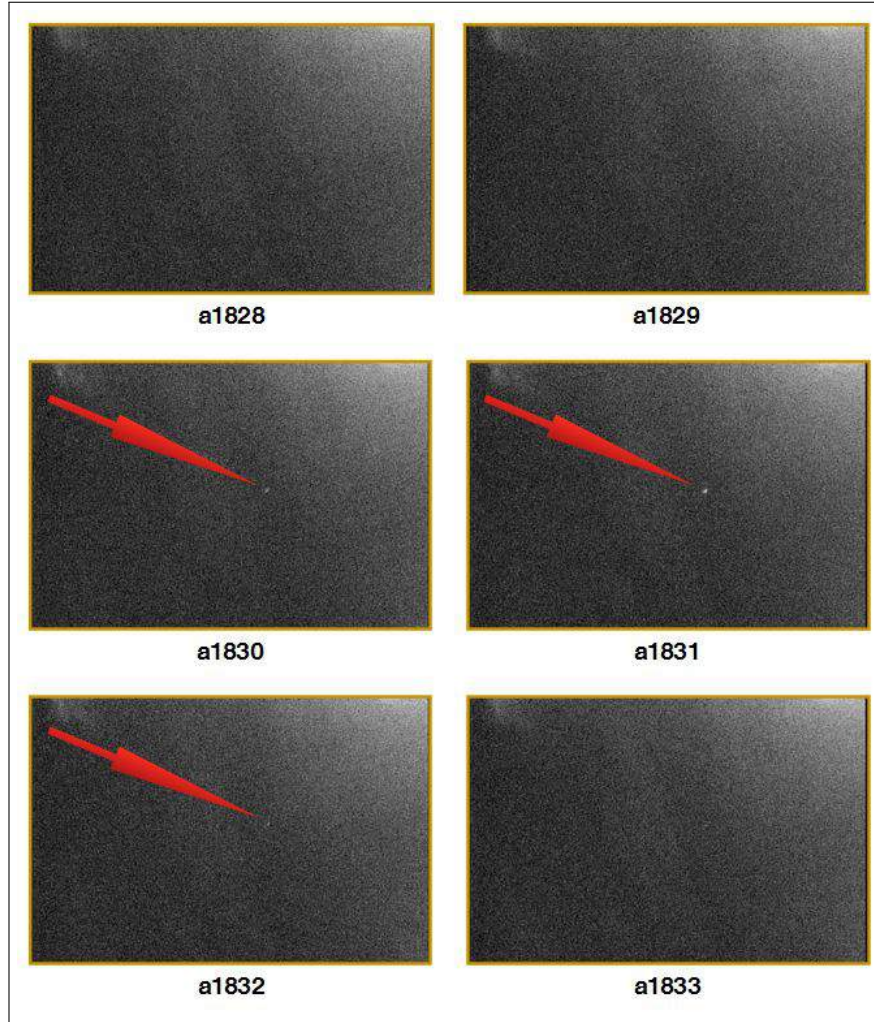


Figure 4.6: LIF captured 19 November 2001, 00:18:58 UTC lasting 0.099 s, Eq.4.51. Flash occurring in frames a1830, a1831 and a1832. Image extracted from footage courtesy of Cook (2014)

time of flash (t_f) is calculated from equation 4.50, taken from equation 4.37. The new parameter IFR = individual flash frames. The third footage that was analysed displayed a flash at the very beginning of the video on March 28th 2220 UTC (no year recorded). The flash lasted for 24 frames (fig. 4.7, fig. 4.8) with the time calculated in equation 4.52. Uncertainties for all three events are an estimate of half a frame rate at 29 FPS.

$$= \frac{(56 \text{ s}) \cdot 2 \text{ f}f}{1702 \text{ f}f} = (0.065 \pm 0.016)\text{s} \quad (4.50)$$

$$= \frac{(108 \text{ s}) \cdot 3 \text{ f}f}{3252 \text{ f}f} = (0.099 \pm 0.016)\text{s} \quad (4.51)$$

$$= \frac{(353 \text{ s}) \cdot 24 \text{ f}f}{8833 \text{ f}f} = (0.959 \pm 0.016)\text{s} \quad (4.52)$$

$$t_f = \frac{VD_L \cdot IFR}{FR} \quad (4.49)$$

Detected Impact Flash 3a

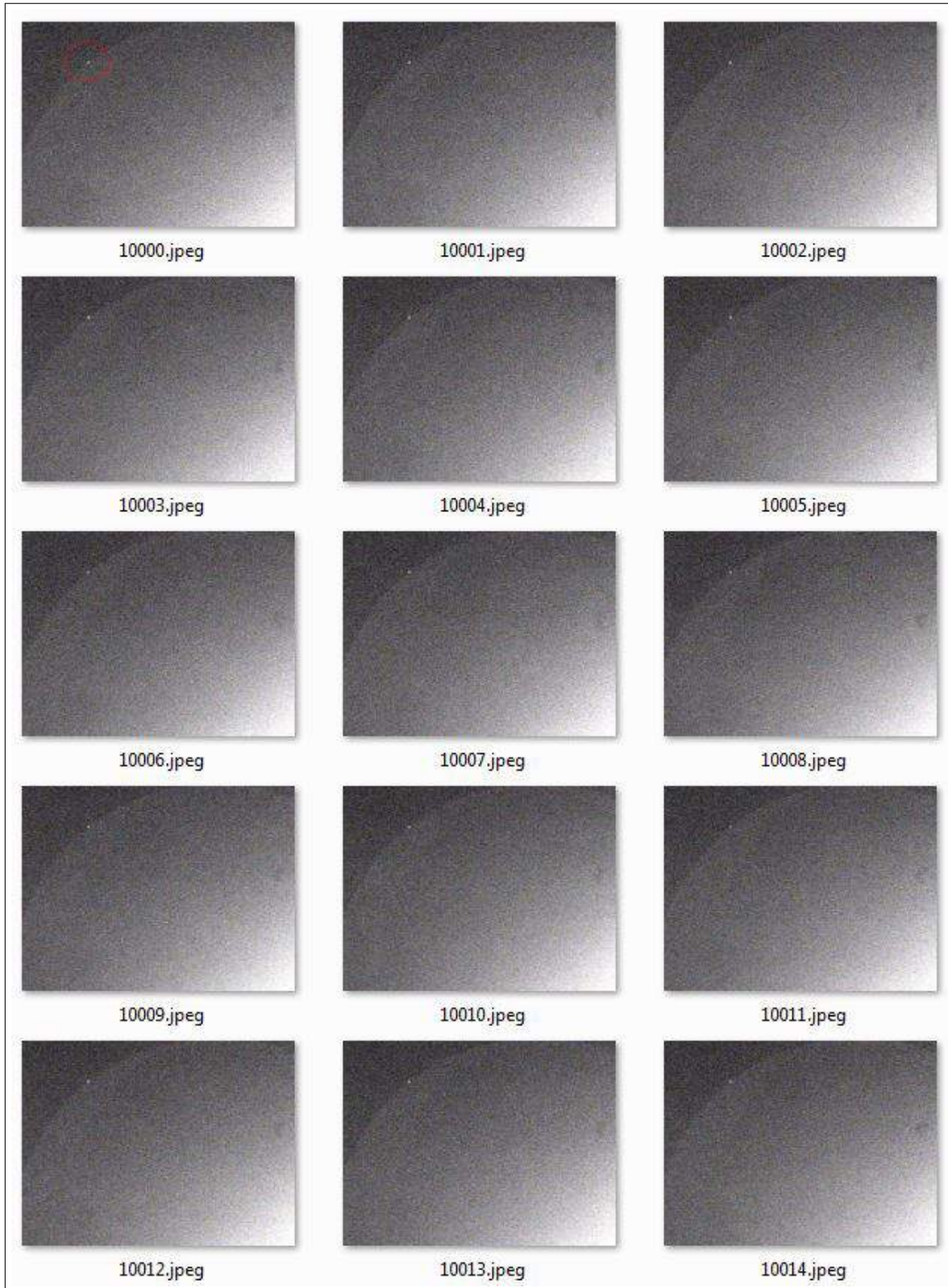


Figure 4.7: A captured flash on the lunar limb at the beginning of the video. The flash starts in frame 1 (1001) and terminates in (1025). The wave band is not known as it was not labelled. Footage taken from archive data, March 28th, UTC 2220. Image extracted from footage courtesy of Cook (2014)

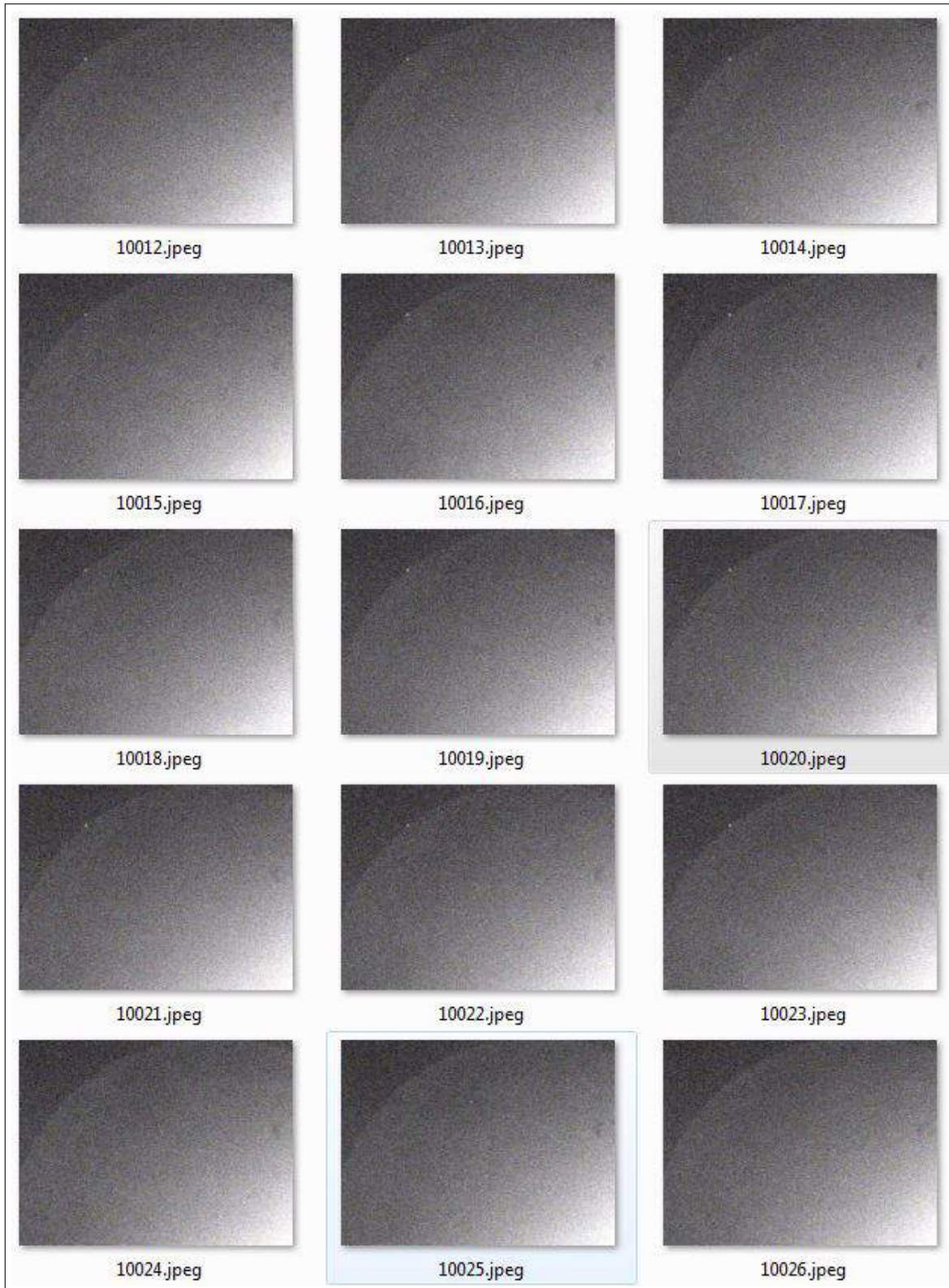
Detected Impact Flash 3b

Figure 4.8: Continued from Detected Impact Flash 3a. Image extracted from footage courtesy of Cook (2014)

Chapter **5**

Discussion

Contents

1	Overall Project Progression	28
2	Cosmic Ray Analysis	28
2.1	Cosmic Ray & Pixel Shapes	28
2.2	The Prominent 'L' Shape	28
2.3	Radial Decrease in Intensity	29
3	Flash Simulation & IFM	29
3.1	Flash Time Considerations	30
4	Detected IFM	31
5	Data Analysis & Software	33
5.1	LunarScan	33
5.2	Registax	33
5.3	Impact Flash Scanner	33
6	Equipment & Hardware	34
7	Background Radiation	34

1 Overall Project Progression

The project took an overall different root from the initial plan, (Appendix C1) due to unexpected and unusual weather. Also, training for Fron Goch telescope was not received as planned and DMAPS domes were often subject to technical difficulties. Per contra, a new objective was established answering questions to what distinguishes the difference between a cosmic ray detection from an IFM. The subordinate question within this project was to conduct a LIF simulation to understand what information can be deduced, in addition to magnitudes. Lastly, subsidiary results were found in relation to the project and discussed within this section.

2 Cosmic Ray Analysis

Distinguishing IFM from cosmic rays are vital in decreasing uncertainties. Many situations can cause scintillation, resulting in false flag IFM. Howbeit, one of the most common candidates are cosmic rays as they have found to occur on average, 5 per minute, eq. 4.45.

To increase certainty that cosmic rays were detected in the experiment and not other attributes, the following was performed. The camera lens was covered and checked for light leaks. Light flashes were tested with the lens cap on to determine if any leaks were occurring. Also, bias-fames were captured at the beginning of each recording to identify and eradicate hot pixels which maybe present. Using Maxlm DL, Douglas (1993) the bias-frame were subtracted from each dark-frame produced by Virtual Dub.

2.1 Cosmic Ray & Pixel Shapes

Dr. Suggs postulated, pixels from an impact flash event would display characteristics of uniformity from a central region. Conversely, pixels excited from cosmic rays have a tendency to occupy single rows, columns or pixels, fig. 5.2, Suggs (2013).

When the main cosmic ray image in figure 5.2 was compared to samples captured from the experiment, only one in sixth samples (020314d) fit the description. The samples display peak intensity at the centre, with the second brightest pixel above and third brightest below the central pixel. This could possibly indicate the pixel's direction of travel before striking the CCD, fig. 5.1. Also the angle of incidence may be the cause of the central brightest pixel relative to the others, with the third brightest pixel resulting in a comic ray 'trail'.

2.2 The Prominent 'L' Shape

Samples 010314d, 280214d, 030314d, 040314d and 270214n share common attributes. There is a central bright pixel and two subordinate pixel, forming an 'L' shape , fig. 5.1. A Likely explanation is the cosmic ray's direction of travel may be at an angle diagonal to the pixel lattice, fig. 5.1. The brightest pixel within the lattice could possibly indicate the initial cosmic ray strike, with surrounding pixels occurring from a residual effect.

Around 500 000 cosmic rays pass through the average person per hour, Norton (2004b), with approximately 8000 per minute and over 100 per second. An assumption is made that this is true for CCDs. Therefore, from equation 4.45, 5 in 8000 cosmic rays are detected by a CCD every minute. Bearing in mind that cosmic rays are travelling in all direction relative to the CCD; the chance of a comic ray particle exactly striking a CCD parallel to the lattice along one axis, fig. 5.1, at a given point in time is relatively small. In the case of the experiment, 1 in 6 cosmic ray samples were in a 'single row' suggesting parallel travel to the CCD lattice. The remaining 5 samples contain the characteristic 'L' shape and are more common, with an occurrence of five sixths. Overall, in support of Dr. Suggs presentation on cosmic ray characteristics, sample 020314d can be used to confirm a , 'single row' detection. Albeit this may be less common than other types. In addition the more common 'L'

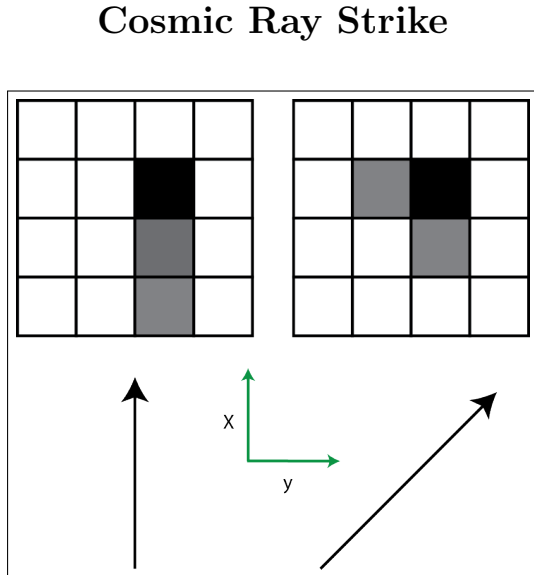


Figure 5.1: A pixel lattice with cosmic rays striking a CCD. On the left is a cosmic ray entering the CCD in the direction of the arrow, along the x-axis. Right, is a cosmic ray entering the CCD along the arrow (diagonally) across both x and y-axis. The black square represents the brightest pixel.

shaped detected cosmic ray may not only be a new characteristic of Dr. Suggs presentation, but may contain a higher frequency of detection.

2.3 Radial Decrease in Intensity

During the impact flash experiment an unexpected flash occurred at frame 1406, 28 s into the video. The flash had a duration of 1 frame, lasting 0.02 s in the V band. Also the event took place 2 s after the main expected experimental flash, with a significant distance between them. Therefore, the unknown event is not associated with the main flash. A bias-frame was captured and rules out any hot pixels, so the only probable explanation is that the unknown source is from a cosmic ray particle. If the unknown source is a cosmic ray particle then this is discordant to Dr. Suggs' presentation stating, an impact event similar to stars are brighter in the center when analysing the pixels of an image, fig. 5.2. The possible cosmic ray flash in figure 5.3 was digitally reproduced, fig. 5.4 and has

the same characteristics as the impact event in figure 5.2.

An explanation is that the likely cosmic ray's angle of incidence was close to 90° . Such an impact perpendicular to the CCD surface may be the cause of an intensity decrease in the radial direction, causing the characteristics of a cross, fig. 5.4. This appears to be rare and was not found in any of the six samples. The lack of time and preparation for assessments prohibited further investigation. However, possible future experiments could be conducted to find the probability of such characteristics, helping ruling out and reduce uncertainties.

3 Flash Simulation & IFM

The flash simulation experiment was an important part to this project as observations were often not permitted. This gives a basic understanding of magnitude calculations and flash collaboration. In the experiment the flash's magnitude was calculated to be -10.6 (Appendix B2) which is close to -10.7 using eq. 4.31. Any calculated uncertainties within the experiment, are for the purpose of scientific demonstration only. This is due to the LED's luminosity inaccuracy and the fact that the experiment was merely a demonstration of procedure. Also (L) in eq. 4.20 would not be estimated in a real event. The calculated magnitude has a reasonable value, as the star Sirius posses a magnitude of -1.44 and would appear fainter if it was in the same frame; given the distance and exposure time. In a real LIF scenario eq. 4.31 would become eq. 5.1, where R = Johnson-Cousins magnitude, k' = extinction coefficient, X = airmass, T = colour response correction term, $(B - V)$ = colour index, R = zero point for the night and $S = DN$ = pixel value 0 - 255, Suggs (2013).

$$R = -2.5 \log(S) - k'X + T(B - V) + ZP \quad (5.1)$$

Event Pixel Comparison

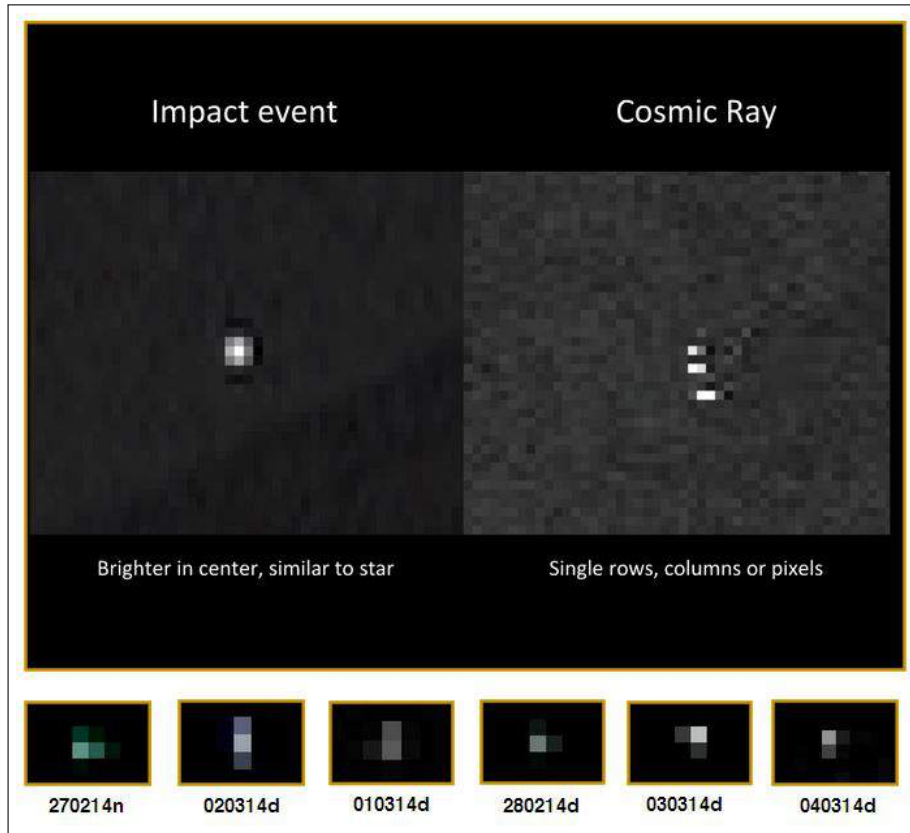


Figure 5.2: An image courtesy of Suggs (2013), comparing pixels from an impact event and cosmic rays. At the bottom are six samples extracted from the cosmic ray experiment. Although it is very difficult to visualise, 5 samples out of 6 contain are 'L' shaped.

From the calculated magnitude, luminous energy (E_{lum}) can be found, eq. 5.2 where, $\Delta\lambda =$ filter half power width, 1607 Ångstroms for R , $f = 2$ for flashes near the lunar surface, $d =$ distance to the Moon from Earth, $t =$ exposure time, and $f_\lambda = 10^{(-R+21.1+zp_R)/2/5}$ where $zpr =$ photometric zero point for R, Suggs (2013).

$$E_{lum} = f_\lambda \Delta\lambda f \pi d^2 t \quad (5.2)$$

$$KE = \frac{E_{lum}}{\eta} \quad (5.3)$$

$$M = \frac{2KE}{v^2} \quad (5.4)$$

$$\eta = 1.5 \times 10^{-3} \exp\left(\frac{-9.3^2}{v^2}\right) \quad (5.5)$$

Using the magnitude equation and luminous energy the kinetic energy (KE) and mass, M can be deduced, eq. 5.3, eq. 5.4, where η is the luminous efficiency (eq. 5.5) and $v =$ velocity, Suggs (2013).

3.1 Flash Time Considerations

The experiment flash's timespan was based on the number of video frames it was detected in. The approximation for EV was established on the fact that the flash could have occurred in

Unknown Flash

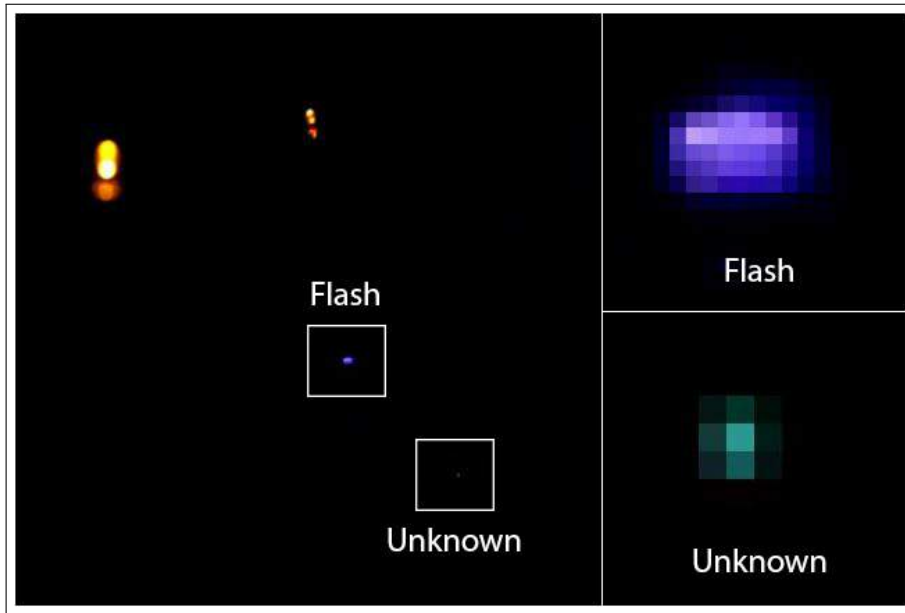


Figure 5.3: Left, a superimposed image of an unknown event within the flash experiment. Right, are both events with increased magnification. Although difficult to see due to print, the unknown pixel occupies 9 pixels with a central cross, Fig. 5.4.

Unknown Flash Pixel Diagram

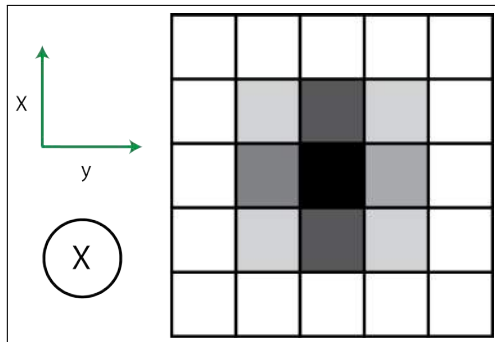


Figure 5.4: A digital representation of an unknown flash in figure 5.3. The \otimes shows the possible direction of a likely cosmic ray candidate going into the paper.

less time than the frame's integration time, but averaged out over the whole frame due to the intensity of the flash. To the contrary, the very beginning or end of the flash where peak light intensity is not yet reached, might not have been detected by the previous or later frame. In this case if the intensity is relatively low, light would be averaged out by the re-

maining darkness thus resulting in very little or no flash detected in either frames.

The CCD's sensitivity to particular wavelengths must be considered within the experiment. Like human eyes, regular cameras unless stated are only sensitive to wavelengths in the optical range; approximately between 400 - 700, Jewett and Serway (2010) . Conversely, modern camera's including the Canon 60D are able to detect wavelengths in the near infra-red . Therefore the exposure time which gives an approximation of the flash's time scale, is for a given waveband. If sensitivity of the CCD was extended far outside of the optical range then the flash's occurrence would be longer.

4 Detected IFM

Detected IFM were compared to the experiment flash to look for any similarities, fig. 5.6. It is imperative at this juncture to draw emphasis on the fact that they are two very differ-

NASA Confirmed IFM

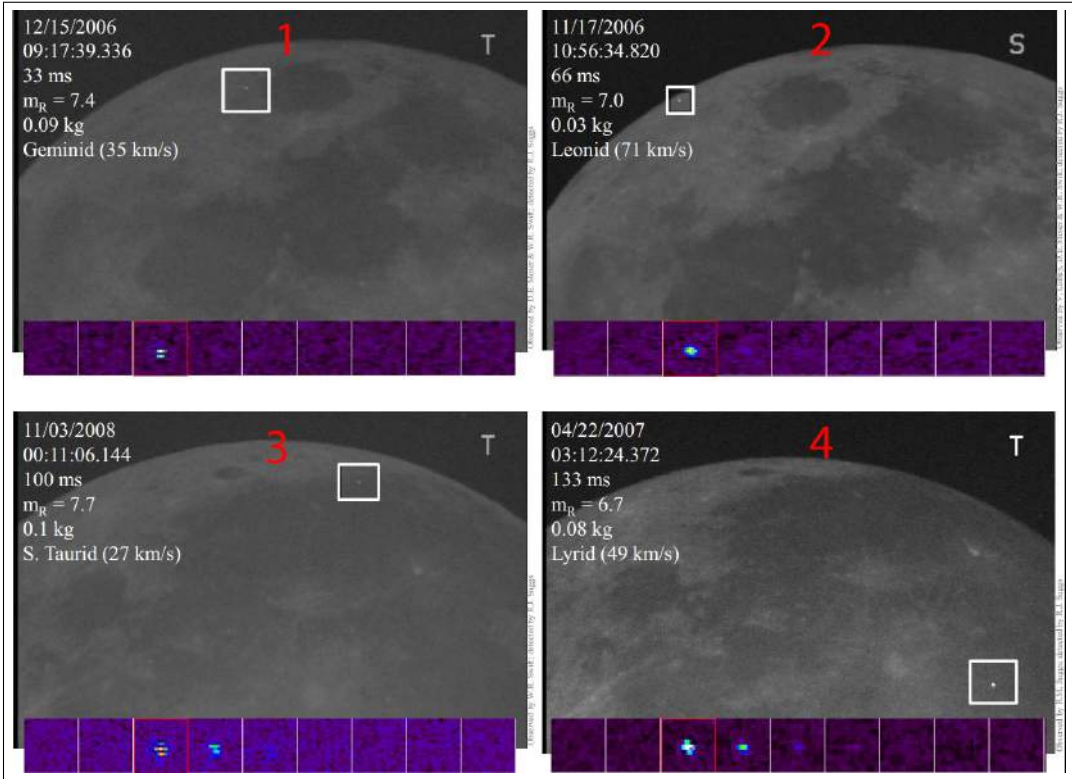


Figure 5.5: Four confirmed LIF events with enhanced pixel view at the bottom of each quadrant, Suggs (2013).

Detected Flash Comparison

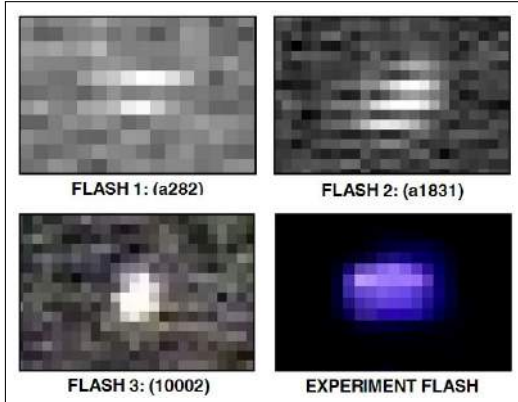


Figure 5.6: Comparison of detected flash 1, 2 and 3 with the experiment flash.

ent types of flashes and may differ in appearance. Nonetheless, there maybe some common traits. Flash 1, 2 and 3, fig. 5.6 are subject

to significant noise, which makes comparison rather difficult. Nevertheless, when compared to the experiment flash it is clear that flash 2 and 3 bear similarity. Namely, common to all three are very strong pixel intensity, adopting a slight elliptical shape. When the experiment flash, flash 2 and 3 are compared to the LIF in quadrant 2, fig. 5.5 they have substantial amounts of resemblance. Looking at fig. 5.5 one can see that IFM can adopt many shapes and characteristics. E.g. the IFM in quadrant 1 appear completely different to quadrant 2. It is nearly the same shape as flash 1, fig. 5.6 with two horizontal lines. Flash 1, is in likeness to quadrant 1 and fig. 5.5 is somewhat different in appearance from it's peers. When analysing quadrant 3 and 4, their contour is the same as what was describe by Suggs (2013). This can be seen and compared to the impact event in figure 5.2, which displays brightness within the central region, decreas-

ing in intensity radially.

When looking at IFM in fig. 5.5 and flashes in fig. 5.6, it is evidently clear that they do not bear any characteristics similar to cosmic ray samples in figure 5.2. To the contrary, quadrant 3, fig. 5.5 resembles the unknown flash, fig. 5.3, which maybe from a cosmic ray particle. Howbeit, due to the rarity of this flash as a cosmic ray particle uncertainties remain high until further suggested experiments are carried out, to determine if these cosmic ray shapes are probable. In addition, it is clear from fig. 5.5 that IFM can adopt different shapes when viewed with increased image magnification.

From scrutinising the flashes in fig. 5.6, flash 1 and 2 are highly likely LIF. However, due to the duration of flash 3 the flash may have occurred from an occulting star. This is also very difficult to distinguish as the flash occurs at the beginning of the footage.

5 Data Analysis & Software

5.1 LunarScan

Using all three software was challenging due to significant technical problems with LunarScan and Impact Flash Scanner. The lack of time in which to resolve this was also a problem. At first there were problems installing and reading videos into LunarScan . This was eventually solved, Appendix A2. LunarScan contained specific issues such as unusually slow processing times (4+ hours per 5 min video). Nonetheless, this may be attributed to computer performance and using remote desktop. Conversely, LunarScan is proficient in detecting IFM and is very sensitive. The program can sometimes be challenging for a novice as it exports data in a file readable by SciLab. In addition the software is very particular in reading video files which must contain an AVI extension. Problems also occur when footage has movement within frames and can be problematic if using a telescope without relatively accurate tracking. LunarScan would be most

suitable for those who record footage using a German equatorial or alt-azimuth with a wedge.

5.2 Registax

Registax is very simple to use when analysing videos for IFM. Like most, the software only allows importing AVI files and can be particular with the codec within the files. On occasions AVI's had to be re-rendered using Virtual Dub which can be time consuming. The program is not specific to certain resolutions such as LunarScan and Impact Flash Scanner, but larger resolutions take longer to process. Processing a 1 minute 720×480 file took around 5 minutes or less. The main hindrance of Registax is the inability to process moving objects within frames, so a telescope with accurate tracking is needed. The out-put file containing a flash is in AVI, and a text file with information of the flash pixel coordinates, deviation and intensity. In addition, the flash video clip is trimmed to contain only the time segment with the flash. The flash is also highlighted and circled yellow which makes the event easy to find. Due to the ease of use, Registax was used for the cosmic ray experiment as there were no moving objects within the frame.

5.3 Impact Flash Scanner

Impact Flash Scanner (IFS) was very difficult to use at first due to problems in the code. The software was built using C++ computer programming language and can be challenging for a novice who has no previous experience in computer programming languages. To operate Impact Flash Scanner, a compiler was installed such as MinGW. Using MinGW, IFS can be exported as an 'exe' file and used by anyone. The program only accepts BMP files, so it can be time consuming to import AVI videos into Virtual Dub and export as a BMP file. Once the BMP files are imported into IFS processing time was relatively rapid.

Frames with flashes detected are presented as outputs with a small box placed around the flash. However, problems were encountered opening BMP files on both DMAPS and other computers. Various programs were used to read the files, but only a black screen would appear when opening the file. It must be emphasized at this stage that such issues are not a result of IFS. To tackle this problem the program's code was changed, Appendix X2 (Lines 368,409 and 432), to read PNG files which were less problematic. With success the PNG files displayed, but problems with displaying the small box around the flash persisted. Numerous attempts were made to rectify this, but despite countless hours trying and the lack of time, the process was unsuccessful.

IFS was particular to only 3 types of resolutions which means that videos had to be converted. Nonetheless, the process can be achieved upon converting the AVI into BMP files. The program can also be very sensitive and yield false impact flash detection. Besides such dilemmas, if the problems are rectified in the future IFS is a proficient and easy to use program that has a major advantage over the others, by reading moving objects within frames. In general, Virtual Dub was often used due to lack of time and ease of use. However, drop frames may occur when using over remote desktop resulting in increased uncertainties.

6 Equipment & Hardware

The equipment at DMAPS are sufficient for detecting IFM, Cain (2010); Cooke et al. (2007) and often work well. However, on occasions technical issues with the dome prevented observations. Automatic tracking could be a problem with the telescope and can lead to difficulties detecting IFM with software. Consequently, manual tracking was used with fine slew speeds. Measures to help tracking accuracy are to first ensure GPS coordinates are accurate for the telescopes location. It is also important that the tracking rate is set to 'lu-

nar'. Other settings would result in the tracking rate being out of synchronisation with the Moon's movement across the sky. For greater tracking accuracy manual star alignment using 3 or more stars further apart from each other should be performed. Auto-align is more straight forward but is less accurate as it usually selects 1-2 stars for alignment. Once aligning using a star, one should ensure the star is central within the view finder.

Greater tracking can be achieved with a German equatorial mount which eliminates field rotation and has smooth tracking, fig. 5.8. An alt-azimuth using a wedge, fig. 5.7 can yield the benefits of a German equatorial mount. Such setup would need a one time polar alignment to Polaris¹ if mounted on a pier. With this accurate tracking would be achieved, see DVD (German Equatorial²). In addition, greater chance of detecting IFM can be accomplished by increasing the field of view. Example in, Appendix C2. To achieve this a focal reducer would need to be attached near the telescope's eyepiece.

7 Background Radiation

The background radiation in Aberystwyth was recorded at $0.14 \mu\text{Sv} \cdot \text{h}^{-1}$. For reference, background radiation in the city of Palmyra was $0.12 \mu\text{Sv} \cdot \text{h}^{-1}$, Shweikani et al. (2012) and Mexico City averaged at $0.09 \mu\text{Sv} \cdot \text{h}^{-1}$, ANSTO (2009). When considering background radiation, 10 % of natural radiation is attributed to cosmic rays, DME (2005). Upon comparing the results of Aberystwyth to the city of Palmyra and Mexico City background radiation appears to be relatively normal. Nonetheless, it must be stated that the dates to figures above were not found and could lead to inaccuracies in the conclusion.

¹Earth's 26,000 year axial precession not taken into account

²CG5 German equatorial mount used. Note slight movement due to accidental touch on the slew key.

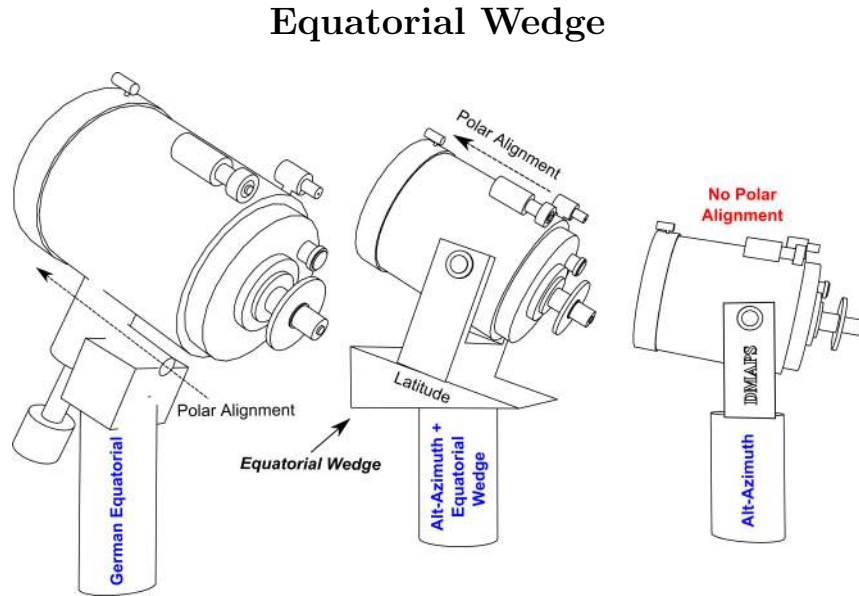


Figure 5.7: Comparison of telescope mounts. Left is a Schmidt-Cassegrain (SCT) Optical Tube Assembly on a German equatorial mount. Right is the telescope at DMAPS on an alt-azimuth mount. Middle is a SCT on an alt-azimuth mount with equatorial wedge. The equatorial wedge allows for accurate tracking and acts like a German equatorial.

Telescope Mounts

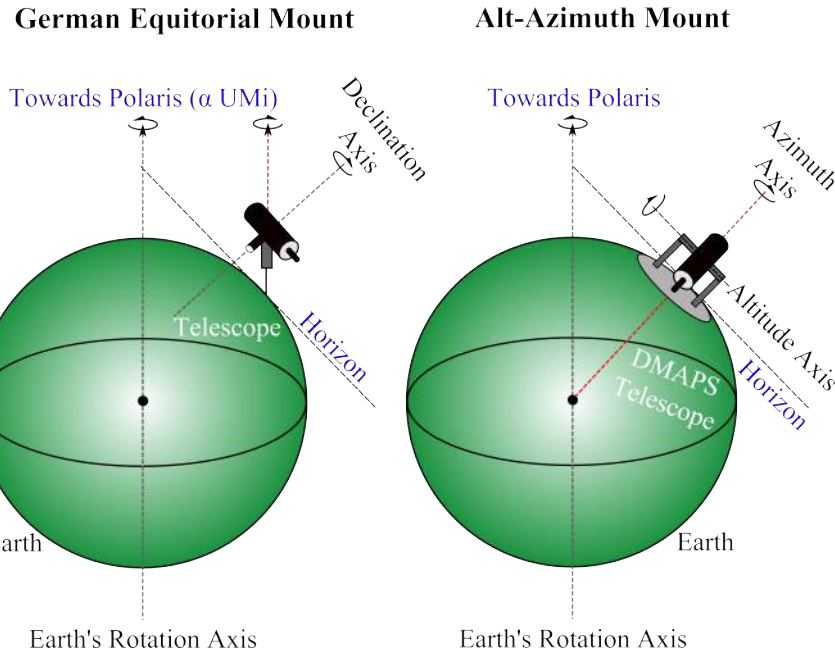


Figure 5.8: On the left is a diagram of a German equatorial mount at some arbitrary location. The mount's right ascension axis is aligned to Polaris with the latitude set to match its current location. The OTA is usually counterbalanced with weights to ensure that the system is well balanced. Such setup allows smooth accurate tracking of celestial objects across the sky. On the right is an alt-azimuth mount setup similar to the observatory at IMAPS. This mount is more straightforward and does not require Polar alignment. The nature of this mount is to allow the OTA to move in steps of up, down, left and right which is the opportunity cost of image field rotation and accurate tracking.

Chapter 6

Conclusion

The main objectives of this project were to analyse characteristics of cosmic ray particles in an image frame, by increasing the zoom until the image becomes pixelated. The other objective was to simulate a LIF by creating a 'dummy flash', gaining better understanding of how information can be extracted and used in a real event.

Five in six cosmic ray samples contained a characteristic 'L' shape. This may suggest the angle of incident relative to the CCD. In accordance to Dr. Suggs claim, a single row/column pixel was found which had a one in six chance of occurring. However, no single pixel cosmic rays were found. The certainty for this is high, as bias frames eliminated hot pixel candidates and light leaks were not present. Also the experiment was conducted in a dark environment with the camera lens cap on. Implications of such results enhance Dr. Suggs claim of single row/column cosmic ray induced pixels. In addition, there is a new 'L' shaped cosmic ray induced pixel not mentioned by Dr. Suggs, Suggs (2013).

A 'dummy flash' was conducted in an experiment which resembled two IFM found in archive data. They contained an elliptical shape with strong pixel intensity. Overall the intensity was strong in the central region which decreased radially and concurs to Dr. Suggs statement.

An unknown flash was detected in the

'dummy' flash experiment which displayed characteristics of intensity in the central region, decreasing radially. Certainty of the 'unknown flash' resulting from a cosmic ray strike are rather high as the same procedures were performed as above. A possible explanation is from cosmic ray strikes perpendicular to the CCD. This would be rather rare and can explain why this type of cosmic ray strike does not appear in the other six samples. The relative magnitude found from the 'dummy' flash was -10.6 mag, which was reasonable. Applying a similar magnitude equation to a real event revealed other information such as luminous energy, kinetic energy, mass and luminous efficiency can be determined from a LIF.

Using all three programs it was found that Impact Flash Scanner had a an advantage of analysing footage with moving objects within frames. However, it needs more work to run correctly. Registax proved user friendly, although it lacks the ability to analyse moving objects within frames. Using techniques from above flash 1 and 2 are highly likely LIF. Although, flash 3 may have occurred from an occulting star. Finally, an experiment could be conducted to investigate the validity of the 'unknown flash'. It's probability of detection could also be determined. The cosmic ray experiment may be improved by increasing the number of data collected, which would reduce uncertainty in the overall result.

Reference

- ANSTO (2009). *The Australian Nuclear Science and Technology Organisation : Ionising Radiation*. Australian Government, pp. 1 - 8.
- Artem'eva, A. N., Kosarev, B. I., Nemchinov, V. I., Trubetskaya, A. I., and Shuvalov, V. V. (1999). Evaluation of light flashes caused by impacts of small comets on the surface of the moon. *Earth, Moon and Planets*, pp. 449-505., 34(6).
- Beiser, A. (1995). *Applied Physics*. McGraw-Hill, Inc, p. 361.
- Bellot Rubio, R. L., Ortiz, L. J., and Sada, V. P. (2000). Observation and interpretation of meteoroids impact flashes on the moon. *Earth, Moon and Planets*, pp. 575-598.
- Berrevoets, C. ((2011)). Available from: <http://www.astronomie.be/registax/index.html>. (Accessed 16 February 2014)).
- Bouley, S., Baratoux, D., Vaubaillon, J., Mocquet, A., Le Feuvre, M., Colas, F., Benkhaldoun, Z., Daassou, A., Sabil, M., and Lognoné, P. (2011). Power and duration of impact flashes on the moon: Implication for the cause of radiation. *Icarus*, pp. 115-124.
- Burchell, J. M., Robin-Williams, R., and Foing, H. B. (2007). Measurements of the surface brightness of the earthshine with applications to calibrate lunar flashes. *The Astronomical Journal*.
- Burchell, J. M., Robin-Williams, R., and Foing, H. B. (2009). The smart-1 lunar impact. *Icarus*, pages 28–38.
- Cain, R. J. (2010). Lunar dust: The hazard and astronaut exposure to risk. *Earth Moon Planets*, 107.
- Carbognani, A. and Cremonese, G. (2002). Excitation and ionization of sodium in meteoroid impacts on the moon. *University of Parma*, pp. 1-5.
- Cinque, S. ((2005)). Available from: <http://www.squared5.com/>. (Accessed 15 February 2014).
- Colin, P. ((2005)). *MinGW*, Available from: <http://www.mingw.org/>. (Accessed 02 March 2014).
- Cook, C. A. (2004). Impact flash scanner. *Aberystwyth University*.

- Cook, C. A. (2012a). Future concepts for impact flash observing. *European Planetary Science Congress*, 7:p. 1.
- Cook, C. A. (2012b). *The Hatfield Lunar Atlas*. Springer, pp. 20 - 21.
- Cook, C. A. (2014). *Department of Mathematics and Physics: Solar System Physics*. Aberystwyth University.
- Cooke, J. W., Suggs, M. R., Suggs, J. R., Swift, R. W., and Hollon, N. (2007). The nasa lunar impact monitoring program. *Earth Moon and Planet*, pp. 293-298.
- Cudnik, B. (2009). *Lunar Meteoroid Impacts: and How to Observe Them*. Springer, p. 111.
- Cudnik, B. ((2013)). *Lunar Meteoroid Impacts Observation and the LADEE Mission Available from: <https://connect.arc.nasa.gov/p4zpsnm6weh/?launcher=false&fcsContent=true&pbMode=normal>*. (Accessed 10 March 2014).
- DME (2005). *Understanding Radioactivity and Radiation in Everyday Life*. Department of Minerals and Energy, Republic of South Africa, p. 8.
- Douglas, B. G. ((1993)). *Maxlm DL*, Available from: <http://www.cyanogen.com/>. (Accessed 26 February 2014).
- Dunbar, B. ((2013)). *NASA*: Available from: http://www.nasa.gov/centers_marshall/news/lunar/index.html. (Accessed 11 March 2014).
- Dunham, B., Cudnik, M. B., Sada, V. P., Melosh, J., Beech, M., Frankenberger, R., Pellerin, L., Venable, R., Asher, D. and Sterner, R., Gotwols, B., Wun, B., and Stockbauer, D. (2000). The first confirmed video recordings of lunar meteor impacts. *Lunar and Planetary Science*, p. 1547.
- EPA ((2013)). *United States Environmental Protection Agency*: Available from: <http://www.epa.gov/radiation/understand/perspective.html>. (Accessed 21 March 2014).
- Gates, M. ((2004)). Available from: <http://www.stellarium.org>. (Accessed 13 February 2014).
- Gural, P. (2007). Automated detection of lunar impact flashes,. Huntsville, Alabama. NASA MSFC.
- Hughes, I. and Hase, P. T. (2009). *Measurements and their Uncertainties*. Oxford University, p. 43.
- Jewett, W. J. and Serway, A. R. (2010). *Physics for Scientists and Engineers with Modern Physics*. Brookes/Cole, p. 998.
- Kutner, L. M. (2003). *Astronomy: A Physical Perspective*. Cambridge University Press, p. 435.
- Madiedo, M. J., Ortiz, L. J., Morales, N., and Cabrera-Canō, J. (2014). A large lunar impact blast on 2013 september 11. *Royal Astronomical Society*.
- Norton, J. A. (2004a). *Observing the Universe*. The Open University, p. 31.
- Norton, J. A. (2004b). *Observing the Universe*. The Open University, p. 60.

- Ortiz, L. J., Sada, V. P., Bellot Rubio, R. L., Aceituno, J. F., Aceituno, J., Gutiérrez, J. P., and Thiele, U. (2000). Optical detection of meteoroidal impacts on the moon. *Astrophys*, pp. 921-923, 405.
- Poje, M., Vukovic, B., Radolic, V., Miklavcic, I., Faj, D., Pajtler, M., and Planinic, J. (2011). Mapping of cosmic radiation dose in croatia. *Elsevier*, pp. 30-33.
- Rasband, W. (2011). Imagej: Available from: <http://imagej.nih.gov/ij/>. (accessed 26 April 2014).
- Roos, M. (2003). *Introduction to Cosmology*. Wiley, p. 42.
- Rothery, A. D., McBride, N., and Glimour, I. (2011a). *Introduction to the Solar System*. Cambridge University Press, p. 36.
- Rothery, A. D., McBride, N., and Glimour, I. (2011b). *Introduction to the Solar System*. Cambridge University Press, p. 134.
- Shweikani, R., Al-Masri, S. M., Hushari, M., Raja, G., and Aissa, R. (2012). Natural radiation background in the ancient city of palmyra. *Elsevier*, pp. 557-560.
- Sridharan, R., Ahmed, M. S., Tirtha Pratim Das, P., Sreelatha, P., and Pradeepkumar, P. (2010). The sunlit lunar atmosphere: A comprehensive study by chance on the moon impact probe of chandrayaan-1. *Planetary and Space Science*, pp. 1567-1577., 58.
- Suggs, R. ((2013)). *Lunar Meteoroid Impacts Observation and the LADEE Mission* Available from: <https://connect.arc.nasa.gov/p4zpsnm6weh/?launcher=false&fcsContent=true&pbMode=normal>. (Accessed 10 March 2014).
- Tipler, A. P. and Mosca, G. (2008). *Physics With Modern Physics for Scientists and Engineers*. W. H. Freeman and Company, p. 1041.
- Tsembelis, K., Burchell, J. M., Cole, J. M., and Margaritis, N. (2008). Residual temperature measurements of light flash under hypervelocity impact. *International Journal of Impact Engineering*, 35.
- Virtual, D. ((2005)). Available from: <http://www.virtualdub.org/>, version. 1.10.14. (Accessed 23 February 2014).
- WordTimeSavers (1998). Available from: <http://www.worldtimeserver.com/atomic-clock/>. (accessed 7 February 2014).
- Yanagisawa, M. and Kisaichi, N. (2002). Lightcurves of 1999 leonid impact flashes on the moon. *Icarus*, pp. 31-38.
- Yanagisawa, M., Ohnishi, K., Takamura, Y., Masuda, H., Sakai, Y., Ida, M., Adachi, M., and Ishida, M. (2006). The first confirmed perseid lunar impact flash. *Icarus*, pp. 489-495.
- Zelik, M. and Gregory, A. S. (1997a). *Introductory Astronomy and Astrophysics*. Brookes/Cole, p. 61.
- Zelik, M. and Gregory, A. S. (1997b). *Introductory Astronomy and Astrophysics*. Brookes/Cole, p. 233.

Glossary

Airmass The path length of light from a celestial source through the Earth's atmosphere in relation to the zenith, that is attenuated by scattering, fig. 2.4.

Astronomical Twilight Sunlight scattering in the upper atmosphere caused when the Sun is 18° below the horizon.

Bias Frames A frame captured by an imaging sensor with bare minimal or no exposure time. Any noise within an image of a bias frame would be due to electronics and not captured photons.

Black Body Continuum Thermal radiation emitted by an object. Such an object is a perfect emitter and absorber of radiation over all wavelengths.

Comets Refers to a small astronomical body composed of rock, dust and ice, in orbit around the Sun.

Cosmic Rays High energy wave/particles that come from space.

Dark side A term used to describe a part of the Moon that is never viewable from Earth as a result of synchronous orbit.

Flux Density A quantity that measures the rate of radiation from an astronomical source, received per unit area.

Luminous Efficiency A measure of how well an object produces visible light.

Meridian An imaginary arc that connects the north celestial pole to the south celestial pole, when passing through the zenith.

Meteor (Shooting Stars) Meteoroids that are burnt up upon entering a celestial atmosphere.

Meteorite Refers to meteoroids that have impacted a celestial body such as a planet, after surviving the intense atmospheric friction.

Meteoroid Small pieces of matter (mainly rock and dust particles), which have broken up from asteroids or ejected by comets.

Noise A grain effect in images that affects quality. Usually this occurs when imaging in low light.

Transient Lunar Phenomenon A relatively short period of change on the surface of the Moon.

Visual Magnitude Also referred to as Apparent magnitude, is the apparent brightness of a body as estimated by the human eye.

Zenith A point directly above and perpendicular to the ground.

Appendices

Appendix A1

Zoomed Focus

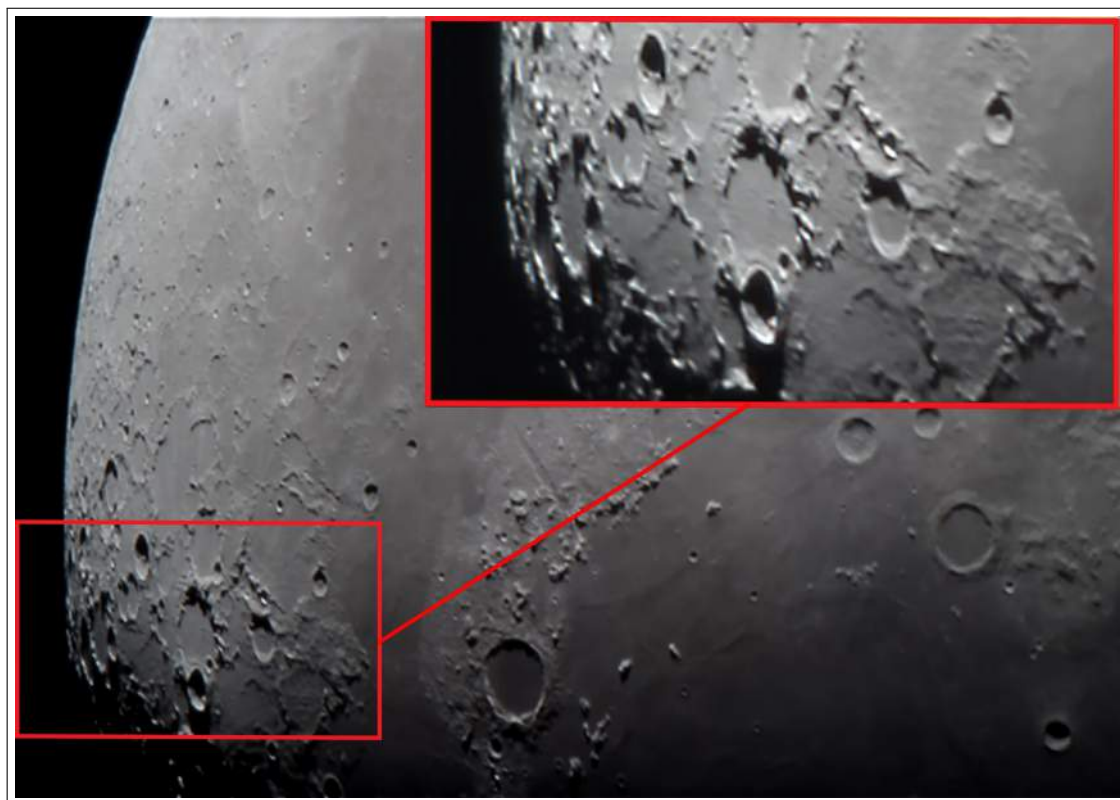


Figure 1: An example of focusing by zooming into a prominent feature. The image above shows a camera zooming into the Crater Goldschmidt. By increasing the zoom the image quality decreases. However, by achieving maximum clarity on the zoomed object generally ensures maximum image quality when zoom is decreased.

Appendix A2

Specific Software Instructions

Problems were encountered using some data analysis software. Therefore specific instructions are detailed below:

LunarScan

- (1) Download and install all associated files into a folder called 'LunarScan' directly on the c drive.
- (2) Create subfolders within LunarScan called 'Data' and 'AVIs'. Then open 'LUNARSETTINGS.txt' file and change the input, output paths to the folders you have just created. 'AVIs' is the input folder.
- (3) Place the avi files in the 'AVI's folder.
- (4) Run LunarScan.exe where you are presented with 5 windows.
- (5) In the command window select option 'P' to make sure the avi file plays ok in LunarScan. If it does not play, import it into to Virtual Dub where you can resize it to 720×480 and export as avi.
- (6) In the LunarScan command window select option '1' and set masking region.
- (7) Select option '3' to find flashes.
- (8) Finally, select option '5' to confirm impact flashes found in the scan.

Appendix B1

Archive data from Dr. T Cook, DMAPS and personal storage were examined using Virtual Dub and LunarScan. Each footage has been analysed, listed and categorised in six tables below. Total footage hours are tallied at the end of each table with the overall grand total of footage time analysed (T) calculated below, where n = total footage time for each table.

$$\begin{aligned} T(\text{hr}) &= \frac{1}{60 \text{ min}} \sum_{n=1}^6 n \\ &= \frac{(119.56 + 181.53 + 171.43 + 273.18 + 64.8 + 444.42) \text{ min}}{60 \text{ min} \cdot \text{hr}^{-1}} \\ &= \frac{1254.92 \text{ min}}{60 \text{ min} \cdot \text{hr}^{-1}} \\ &= 21.32 \text{ hr} \end{aligned}$$

The total footage time analysed was 21 hours and 32 minutes, mostly using Virtual Dub. Each video was scrutinised frame by frame to increase the chance of detecting an impact event, cosmic ray or scintillation.

Analysing Pengdome Archive Data for Impact Flashes 1

File Name	Folder	Method	Time min:sec	Flash	Frame	Total Frames	Note
20120405	April	VD	4:22	0	0	6566	D
30th Jan 2000	Jan	VD	6:16	0	0	9406	NGS
30th Jan 2010	Jan	VD	3:19	0	0	9406	NGS
30th Jan 1908	Jan	VD	4:59	0	0	7498	NGS
29th feb 1855	Feb	VD	4:46	0	0	7167	NGS
29th feb 1900	Feb	VD	4:59	0	0	7499	NGS
29th feb 1914	Feb	VD	4:59	0	0	7499	NG
29th feb 1920	Feb	VD	4:59	0	0	7498	NG
29th feb 1926	Feb	VD	5:07	0	0	7683	NGS
29th feb 1933	Feb	VD	4:59	0	0	7499	NGS
29th feb 1940	Feb	VD	4:59	0	0	7499	N
29th feb 1949	Feb	VD	4:59	0	0	7498	NG
29th feb 2002	Feb	VD	4:59	0	0	7499	NG
29th feb 2008	Feb	VD	4:59	0	0	7499	NGS
29th feb 2014	Feb	VD	4:59	0	0	7499	NS
29th feb 2025	Feb	VD	4:59	0	0	7498	N
19th nov 3am c	Nov	VD	1:28	0	0	2213	GS
19th nov 4am cd	Nov	VD	4:59	0	0	7499	G
19th nov 305 cd	Nov	VD	5:26	0	0	8151	GS
19th nov 315 c	Nov	VD	6:46	0	0	10151	GS
19th nov 325 c	Nov	VD	5:40	0	0	8503	N
19th nov 345 c	Nov	VD	4:59	0	0	7499	N
19th nov 351 c	Nov	VD	5:23	0	0	8094	N
19th nov 408 c	Nov	VD	5:38	0	0	8472	NGS
30th jan 2000	Jan	VD	3:19	0	0	9406	NGS
30th jan 1908	Jan	VD	4:59	0	0	7498	GS
		Total	119.56				

Table 1: VD = Virtual Dub, N = Noisy, G = Significant Glare, S = Lunar dark side with appearance of the day side in frame, T = Accurate tracking, U = Unstable footage and D = Day side only.

Analysing Pengdome Archive Data for Impact Flashes 2

File Name	Folder	Method	Time min:sec	Flash	Frame	Total Frames	Note
4th march 2009 Na	Mar	VD	4:59	0	0	7499	D
4th march 2021 Na	Mar	VD	4:20	0	0	6509	NUD
4th march 2036 Na	Mar	VD	4:20	0	0	6509	NUD
4th march 2042 Na	Mar	VD	4:59	0	0	7498	NUD
4th march 2048 Na	Mar	VD	5:53	0	0	8832	NUD
12304UT201748-Na	Mar	VD	2:52	0	0	4318	UD
5th march 2024 Na	Mar	VD	5:53	0	0	8833	UD
5th march 2315 Na	Mar	VD	5:53	0	0	8832	UD
5th march 2333 Na	Mar	VD	4:59	0	0	7499	UD
5th march 2350 Na	Mar	VD	5:53	0	0	8833	UD
5th march 2357 Na	Mar	VD	4:59	0	0	7499	UD
6th march 2258 Na	Mar	VD	4:25	0	0	6641	UD
7th march 2136	Mar	VD	4:59	0	0	7499	UD
7th march 2145 Na	Mar	VD	4:59	0	0	7499	UD
7th march 2145 Na	Mar	VD	5:53	0	0	8833	N
7th march 2201 na	Mar	VD	5:53	0	0	8833	N
7th march 2211 na	Mar	VD	5:53	0	0	8833	N
7th march 2218 na	Mar	VD	5:53	0	0	8833	N
7th march 2227 na	Mar	VD	5:53	0	0	8833	ND
7th march 2236 na	Mar	VD	5:53	0	0	8832	D
7th march 2247 na	Mar	VD	5:53	0	0	8832	GD
7th march 2253 na	Mar	VD	5:53	0	0	8832	GD
7th march 2300 na	Mar	VD	5:53	0	0	8832	GD
25th march 2056	Mar	VD	4:59	0	0	7499	NS
25th march 2104	Mar	VD	4:59	0	0	7499	N
25th march 2111	Mar	VD	5:53	0	0	8833	NS
25th march 2118	Mar	VD	5:53	0	0	8833	NS
25th march 2123	Mar	VD	5:53	0	0	8833	N
25th march 2129	Mar	VD	5:53	0	0	8833	N
march 26th 1948	Mar	VD	2:45	0	0	4127	NS
march 26th 1952	Mar	VD	5:53	0	0	8833	NS
march 26th 2000	Mar	VD	5:53	0	0	8833	NS
march 26th 2007	Mar	VD	5:53	0	0	8833	NS
march 26th 2018	Mar	VD	5:53	0	0	8833	NS
march 26th 2025	Mar	VD	5:53	0	0	8833	NS
march 26th 2030	Mar	VD	5:53	0	0	8833	NS
		Total	181.53				

Table 2: VD = Virtual Dub, N = Noisy, G = Significant Glare, S = Lunar dark side with appearance of the day side in frame, T = Accurate tracking, U = Unstable footage and D = Day side only.

Analysing Pengdome Archive Data for Impact Flashes 3

File Name	Folder	Method	Time min:sec	Flash	Frame	Total Frames	Note
27th1952	Mar	VD	5:53	0	0	8832	NS
27th2014	Mar	VD	5:53	0	0	8833	NS
27th2019	Mar	VD	5:53	0	0	8833	NS
27th2026	Mar	VD	5:53	0	0	8833	NS
27th2033	Mar	VD	5:53	0	0	8833	NS
27th2038	Mar	VD	5:53	0	0	8833	NS
27th2045	Mar	VD	5:53	0	0	8832	NS
27th2045	Mar	VD	5:53	0	0	8833	NS
27th2056	Mar	VD	5:53	0	0	8833	NS
27th2103	Mar	VD	5:53	0	0	8833	NS
27th2108	Mar	VD	5:53	0	0	8833	NS
27th2117	Mar	VD	5:53	0	0	8832	NS
27th2124	Mar	VD	5:53	0	0	8833	NS
27th2129	Mar	VD	5:53	0	0	8832	NS
27th2137	Mar	VD	5:53	0	0	8833	NS
27th2147	Mar	VD	5:53	0	0	8833	NS
28th 2124	Mar	VD	5:53	0	0	8833	GS
28th 2130	Mar	VD	5:53	0	0	8833	GS
28th 2139	Mar	VD	5:53	0	0	8833	GS
28th 2145	Mar	VD	5:53	0	0	8833	GS
28th 2152	Mar	VD	5:53	0	0	8833	GS
28th 2159	Mar	VD	5:53	0	0	8832	GS
28th 2206	Mar	VD	5:53	0	0	8833	GS
28th 2212	Mar	VD	5:53	0	0	8833	GS
28th 2220	Mar	VD	5:53	1	1-24	8833	GS
28th 2226	Mar	VD	5:53	0	0	8833	GS
29th 2134	Mar	VD	5:53	0	0	8832	GS
29th 2147	Mar	VD	5:53	0	0	8832	GS
29th 2154	Mar	VD	5:53	0	0	8832	GS
29th 2210	Mar	VD	5:53	0	0	8832	GS
29th 2250	Mar	VD	5:53	0	0	8832	GS
		Total	171.43				

Table 3: VD = Virtual Dub, N = Noisy, G = Significant Glare, S = Lunar dark side with appearance of the day side in frame, T = Accurate tracking, U = Unstable footage and D = Day side only.

Analysing Archive Data for Impact Flashes

File Name	Folder	Method	Time min:sec	Flash	Frame	Total Frames	Note
25th march 2104.00	Daf	VD	1:31	0	0	2275	N
25th march 2104.01	Daf	VD	1:31	0	0	2275	N
25th march 2104.02	Daf	VD	1:31	0	0	2275	NG
25th march 2104.03	Daf	VD	0:36	0	0	674	NG
27032103.00	Daf	VD	1:31	0	0	2275	N
27032103.01	Daf	VD	1:31	0	0	2275	N
27032103.02	Daf	VD	1:31	0	0	2275	N
27032103.03	Daf	VD	1:20	0	0	2008	N
27032108.00	Daf	VD	1:31	0	0	2275	N
27032108.01	Daf	VD	1:31	0	0	2275	N
27032108.02	Daf	VD	1:31	0	0	2275	N
27032108.03	Daf	VD	1:20	0	0	2008	N
27032108.00	Daf	VD	1:31	0	0	2275	N
27032117.01	Daf	VD	1:31	0	0	2275	N
28032032.00	Daf	VD	1:15	0	0	2275	N
28032032.01	Daf	VD	1:15	0	0	2275	N
28032032.02	Daf	VD	1:15	0	0	2275	N
28032032.03	Daf	VD	1:12	0	0	2165	N
28032038.00	Daf	VD	1:15	0	0	2275	N
28032038.01	Daf	VD	1:15	0	0	2275	N
28032038.02	Daf	VD	1:15	0	0	2275	N
28032043.03	Daf	VD	1:12	0	0	2275	NG
2210UTC 19072013	Personal	L	70:45	0	0	-	TS
2200UTC 19072013	Personal	L	67:23	0	0	-	TS
2203UTC 19072013	Personal	L	50:10	0	0	-	TS
2208UTC 19072013	Personal	L	57:02	0	0	-	TS
001858UT	Archive	VD	1:48	1	1831	3252	N
231915UT	Archive	VD	0:56	1	283	1702	UNG
		Total	273.18				

Table 4: VD = Virtual Dub, L = LunarScan, N = Noisy, G = Significant Glare, S = Lunar dark side with appearance of the day side in frame, T = Accurate tracking, U = Unstable footage and D = Day side only.

Analysing Dr. Cook's Archive Data for Impact Flashes 1

File Name	Method	Time min:sec	Flash	Frame	Note
a.00	VD	2:16	0	3413	TS
a.01	VD	2:16	0	3413	TS
a.02	VD	2:16	0	3413	TS
a.03	VD	2:16	0	3413	TS
a.04	VD	2:16	0	3413	TS
a.00v	VD	2:16	0	3413	TS
a.01v	VD	2:16	0	3413	TGS
a.02v	VD	2:16	0	3413	TGS
a.03v	VD	2:16	0	3413	TGS
a.04v	VD	2:16	0	3413	TGS
a.05v	VD	2:16	0	3413	TGS
a.06v	VD	2:16	0	3413	TGS
a.07v	VD	2:16	0	3413	TGS
a.08v	VD	2:16	0	3413	TGS
a.09v	VD	2:16	0	3413	TGS
a.10v	VD	2:16	0	3413	TGS
a.11v	VD	2:16	0	3413	TGS
a.12v	VD	2:16	0	3413	TGS
a.13v	VD	2:16	0	3413	TGS
a.14v	VD	2:16	0	3413	UGS
a.15v	VD	2:16	0	3413	NTGS
a.16v	VD	2:16	0	3413	NTGS
a.17v	VD	2:16	0	3413	NTGS
a.18v	VD	2:16	0	3413	NUGS
a.19v	VD	2:16	0	3413	NDGS
a.20v	VD	2:16	0	3413	NTGS
a.21v	VD	2:16	0	3413	NTGS
a.22v	VD	2:16	0	3413	NUGS
a.23v	VD	2:16	0	3413	NUGS
a.24v	VD	2:16	0	3413	NU
	Total	64.8			

Table 5: VD = Virtual Dub, N = Noisy, G = Significant Glare, S = Lunar dark side with appearance of the day side in frame, T = Accurate tracking, U = Unstable footage and D = Day side only.

Analysing Dr. Cook's Archive Data for Impact Flashes 2

File Name	Method	Time min:sec	Flash	Note
2011May09UT212936-213436-WL	VD	4:59	0	NU
2011May09UT213716-214301-WL	VD	5:31	0	GUS
2011May09UT214421-215409-WL	VD	9:33	0	GUS
2011May09UT215625-220125-WL	VD	4:59	0	US
2011May09UT220246-220758-WL	VD	4:59	0	GUS
2012Feb25UT181649-182141-WL	VD	4:50	0	GUS
2012Feb25UT182637-185059-WL	VD	24:20	0	NGUS
Tape187 2009-03-23-00-01-38-185059-WL	VD	9:05	0	DNGUS
Tape134 2009-03-29-14-16-48	VD	61:48	0	DNGUS
Tape135a 2009-03-29-13-09-44	VD	61:47	0	DNGUS
Tape135 2009-03-29-12-02-15	VD	61:50	0	DNGUS
Tape138 2001Nov22-2002Jan18	VD	51:49	0	DNGUS
Tape144-2009-03-18-00-20-16	VD	61:46	0	DNGUS
Tape145 2009-03-17-21-41-4	VD	19:55	0	DNGUS
Tape146 2009-03-18-23-20-19	VD	61:31	0	DNGUS
Total		444.42		

Table 6: VD = Virtual Dub, N = Noisy, G = Significant Glare, S = Lunar dark side with appearance of the Day side in frame, T = Accurate tracking, U = Unstable footage and D = Day side only.

Appendix B2

Experiment Flash Calculation

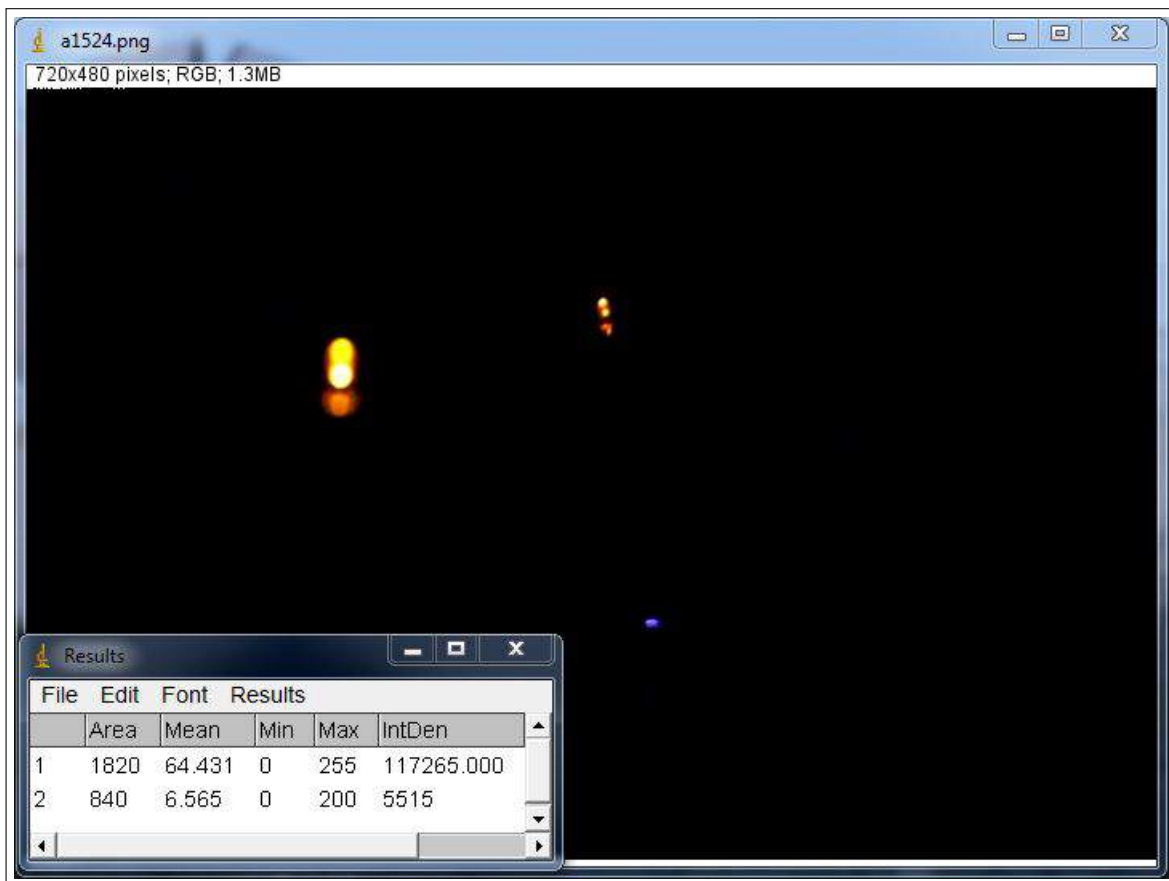


Figure 2: The integration density (IntDen) was found for L1 (1) and the experiment flash (F_*), (2) using ImageJ, Rasband (2011)

The integration density of L1 and the flash was found using a Java-based image processing program called ImageJ, Rasband (2011). With this and knowing the magnitude m_1 from eq. 4.25, the relative magnitude (m_{R*}) of the experiment flash was calculated to be -10.6. This is very close to the estimated value of -10.7, eq. 4.31. The uncertainty is not calculate as explained in the results and discussion section.

$$m_{R*} = m_1 + 2.5 \log \left(\frac{L1}{F_*} \right) \quad (1)$$

$$= m_1 + 2.5 \log \left(\frac{\text{IntDen}(1)}{\text{IntDen}(2)} \right) \quad (2)$$

$$= -13.9 + 2.5 \log \left(\frac{117265}{5515} \right) \quad (3)$$

$$= \boxed{-10.6 \text{ to 3 s.f.}} \quad (4)$$

Appendix C1

Project Plan

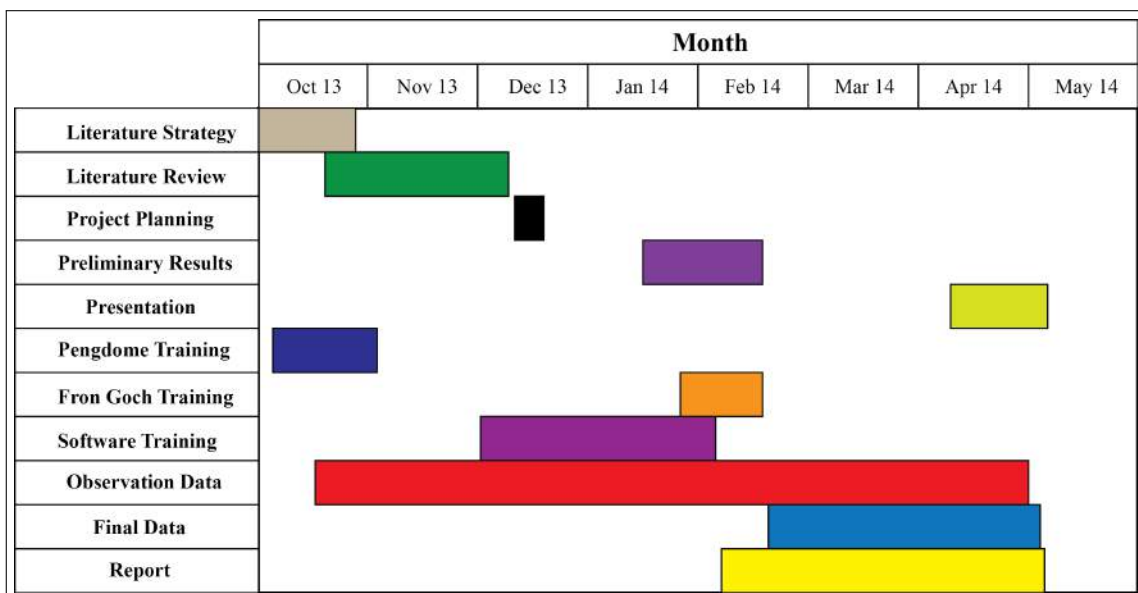


Figure 3: A gantt chart of the project plan starting in October 2013 until May 2014.

Appendix C2

F/6.3 Focal Reducer Derivation

The focal reducer essentially reduces focal length f_o of the telescope, thus increasing the field of view. Knowing the F-number the new f_o can be determined and then from this, find the FOV.

First to start with an equation for the F-number where, $\lambda = 6.3$ is the number, $D_o = 254$ mm is the aperture and f_o is the focal length:

$$F/\lambda = \frac{\text{Focal Length}}{\text{Aperture}} = \frac{f_o}{D_o}$$

Now to solve for, f_o by transposing the equation:

$$f_o = (F/\lambda) \cdot D_o$$

$$= 6.3 \cdot (254 \text{ mm})$$

$$= 1600 \text{ mm}$$

From finding f_o this can be place into the equation that finds the angular field of view (θ_{FR}) with a F/6.63 focal reducer:

$$\begin{aligned}
\theta &= \frac{d_{CCD}}{f_o} = \frac{12.9 \text{ mm}}{1.6 \times 10^3 \text{ mm}} \\
&= 8.06 \times 10^{-3} \text{ rad} \\
&= 8.06 \times 10^{-3} \text{ rad} (180/\pi) \text{ deg} \cdot \text{rad}^{-1} \\
&= 0.461 \text{ deg} \\
&= [0.46^\circ \text{ to 2 s.f.}]
\end{aligned}$$

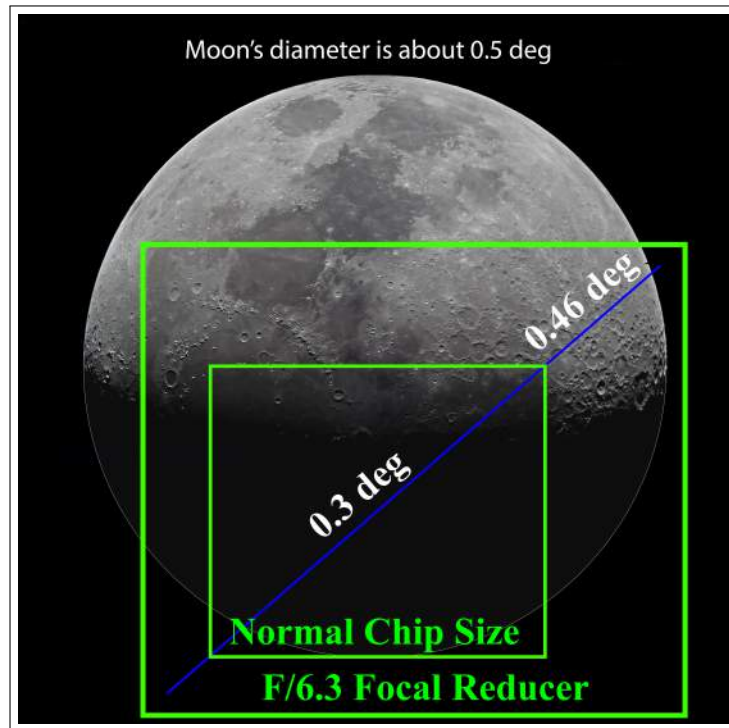


Figure 4: An example of FOV for normal chip-size eq. 3.9 and with a F/6.3 focal reducer in place. The FOV if not exactly to scale but give an idea of the difference.

Appendix X1

Risk Assessment

Brief Description of Activity:	Assessor:	Date:
Lunar impact flash using remotely controlled telescopes	Andre Munoz	11/12/2013

Hazard	Risk	Risk Factor	Control Measures	Residual Risk
Fire from dome lights.	Department	Low	Check lights are off	Very low
Electric shock from lab experiment.	Individual	Low	Keep water away from electrics	Very low

Table 7: Risk assessment of both experiment and observations.

Appendix X2

Impact Flash Scanner C++ Code

Impact Flash Scanner courtesy of Dr. Tony Cook, Cook (2004), edited by the author.

```
-----  
1 #include <stdio.h>  
2 #include <stdlib.h>  
3 #include <cmath>  
4  
5 #define MIN_FLASH_LIMIT 1  
6 #define MAX_FLASH_LIMIT 5  
7 // The min/max number of flash detections in an image before we decide to  
8 // reject that image - this allows us to ignore the bright area of the Moon  
9  
10#define NEIGHBOUR_SD 3 // Define how many S.D. a pixel must be above its  
11// neighbours (over all TV frames) to be flagged up as a possible flash  
12  
13#define TIME_SD 5  
14// No of sd above the mean in the time domain for a flash pixel, and  
15// its neighbour, to the immediate right  
16  
17#define MIN_SD1 4 // If sd of neighbouring pixels in all time domains  
18// smaller than this set the sd to be this - for double_check routine  
19#define MIN_SD2 4 // For flash_detector routine  
20// If sd of neighbouring pixels in all time domains  
21// smaller than this set the sd to be this  
22  
23// Looks for impact flashes on the Moon - uses a real-time  
24// running average and S.D. which do not need to be re-initialized  
25  
26// 2004 Nov 30 - Author: Tony Cook - University of Nottingham  
27// 2014 Mar 31 Edited by: Andre Munoz - Aberystwyth University  
28  
29void sum_average(unsigned char *pixels, long int NPIXELS, double* &avg)  
30{  
31    int ival;  
32    int i,k;  
33    for (i=0;i<NPIXELS;i++)  
34    {  
35        avg[i]=0;  
36        for (k=0;k<60;k++)  
37        {  
38            ival=(int)(*(pixels+NPIXELS*k+i));
```

```

39     avg[i]=avg[i]+ival;
40   }
41 }
42 }
43
44 void sum_sd(unsigned char *pixels, long int NPIXELS, double *mean,
45 double* &sd)
46 {
47   double number;
48   int i,k;
49   for (i=0;i<NPIXELS;i++)
50   {
51     sd[i]=0.0;
52     for (k=0;k<60;k++)
53     {
54       number=(mean[i]/60.0-*(pixels+NPIXELS*k+i));
55       sd[i]=sd[i]+number*number;
56     }
57   }
58 }
59 double get_mean(unsigned char *pixels, int i, int j, int
60 ipos, long int NPIXELS,int NS)
61 {
62   double mean;
63   int ival;
64   int k;
65   mean=0;
66   for (k=0;k<60;k++)
67   {
68     ival=(int)(*(pixels+NPIXELS*k+j*NS+i));
69     if (k!=ipos) mean=mean+ival;
70   }
71   mean=mean/59.0;
72   return mean;
73 }
74
75 double get_sd(unsigned char *pixels, int i, int j, int ipos,
76 double mean,long int NPIXELS,int NS)
77 // Returns the s.d. of all the time frames at a given pixel
78 // position - excluding the time frame we are currently at.
79 {
80   double sum;
81   double x;
82   double sd;
83   int ival;
84   int k;
85   sum=0;
86   for (k=0;k<60;k++)
87   {
88     ival=(int)(*(pixels+NPIXELS*k+j*NS+i));
89     x=ival-mean;
90     if (k!=ipos) sum=sum+x*x;
91   }
92   sd=sqrt(sum/58.0);
93   return sd;
94 }
95
96 int double_check(unsigned char *pixels, int ii, int
97 jj,int ipos,long int NPIXELS, int NS)
98 {

```

```

99     int i,j,k;
100    int id;
101    int ival;
102    int icky;
103    double mean;
104    double count;
105    double diff;
106    double sd;
107    double x;
108
109    mean=0;
110    count=0;
111    // Finds the mean of all the 3x3 pixels centred on the test
112    // pixel in all time frames excluding the test time frame.
113    // Takes into account interlace
114    for (k=0;k<60;k++)
115    {
116        for (j=jj-2;j<=jj+2;j=j+2)
117        {
118            for (i=ii-1;i<=ii+1;i++)
119            {
120                if (k!=ipos)
121                {
122                    ival=*(pixels+NPIXELS*k+j*NS+i);
123                    mean=mean+ival;
124                    count=count+1;
125                }
126            }
127        }
128    }
129    mean=mean/count;
130
131    // Finds the mean of all the 3x3 pixels centred on the
132    //test pixel in all time frames
133    // excluding the test time frame
134    sd=0;
135    count=0;
136    for (k=0;k<60;k++)
137    {
138        for (j=jj-2;j<=jj+2;j=j+2)
139        {
140            for (i=ii-1;i<=ii+1;i++)
141            {
142                if (k!=ipos)
143                {
144                    ival=(*pixels+NPIXELS*k+j*NS+i));
145                    x=ival-mean;
146                    sd=sd+x*x;
147                    count=count+1;
148                }
149            }
150        }
151    }
152    sd=sqrt(sd)/(count-1);
153
154    diff=(*pixels+NPIXELS*ipos+jj*NS+ii))-mean;
155    if (sd<MIN_SD1) sd=MIN_SD1;
156    id=(int) *(pixels+NPIXELS*ipos+jj*NS+ii);
157
158    if (diff>(NEIGHBOUR_SD*sd))

```

```

159     {
160         return 1;
161     }
162     return 0;
163 }
164
165
166
167 int flash_detector(unsigned char* &pixels, unsigned char *&pixies,
168 long int NPIXELS, int ipos, int NS, int NL, double* avg,
169 double* sd, int* flash_count)
170 {
171     int i,ii;
172     int ip1,ip2,ip3;
173     int i1;
174     int di,dj;
175     int j,jj;
176     int k;
177     int ival;
178     double mean1,mean2;
179     double x,y;
180     double sum;
181     double sd1,sd2;
182     double diff;
183
184     *flash_count=0;
185
186 // This fills up the output array with the current 3 input frames
187 for (j=0;j<NPIXELS;j++)
188 {
189     ip1=ipos-1;
190     if (ip1<0) ip1=59;
191     ip2=ipos;
192     ip3=ipos+1;
193     if (ip3>59) ip3=0;
194     *(pixies+j+NPIXELS*0)=*(pixels+NPIXELS*ip1+j);
195     *(pixies+j+NPIXELS*1)=*(pixels+NPIXELS*ip2+j);
196     *(pixies+j+NPIXELS*2)=*(pixels+NPIXELS*ip3+j);
197 }
198
199
200 for (j=10;j<(NL-10);j++) // for loop <1>
201 {
202     for (i=10;i<(NS-10);i++) // for loop <2>
203     {
204         sd1=(*(pixels+NPIXELS*ipos+j*NS+i))-avg[i+j*NS]/59.0;
205         sd1=sqrt((sd[i+j*NS]-sd1*sd1)/58.0);
206         mean1=(avg[i+j*NS]-(*(pixels+NPIXELS*ipos+j*NS+i)))/59.0;
207         //sd1=get_sd(pixels,i,j,ipos,mean1,NPIXELS,NS);
208         if (sd1<MIN_SD2) sd1=MIN_SD2; // make sure we have a sizable s.d.
209         x=mean1; y=sd1;
210         ival=(int)(*(pixels+NPIXELS*ipos+j*NS+i));
211         diff=ival-mean1;
212         if (diff<0)
213         {
214             diff=-sqrt(diff*diff);
215         }
216         else
217         {
218             diff=sqrt(diff*diff);

```

```

219     }
220     diff=sqrt(diff*diff);
221     if ((diff>(TIME_SD*sd1)) && ((mean1>5) && (mean1<250)))
222     // avoids saturation issue
223     {
224     i1=i+1; // checks pixel to the right
225     sd2=(*(pixels+NPIXELS*iPos+j*NS+i1))-avg[i1+j*NS]/59.0;
226     sd2=sqrt((sd[i1+j*NS]-sd2*sd2)/58.0);
227     mean2=(avg[i1+j*NS]-(*(pixels+NPIXELS*iPos+j*NS+i1)))/59.0;
228     //sd2=get_sd(pixels,i1,j,iPos,mean2,NPIXELS,NS);
229     if (sd2<MIN_SD2) sd2=MIN_SD2;
230     ival=(int)(*(pixels+NPIXELS*iPos+j*NS+i1));
231     diff=ival-mean2;
232     if (diff<0)
233     {
234     diff=-sqrt(diff*diff);
235     }
236     else
237     {
238     diff=sqrt(diff*diff);
239     }
240     if ((diff>(TIME_SD*sd2)) && ((mean2>5) && (mean2<250))) // if <2>
241     {
242     if (double_check(pixels,i,j,iPos,NPIXELS,NS)) // if <3>
243     {
244     *flash_count=*flash_count+1;
245     for (dj=-10; dj<=10; dj++) // for loop <3>
246     {
247     for (di=-10; di<=10; di++) // <for loop <4>
248     {
249     if (((di== -10) || (di==10)) || ((dj== -10) || (dj==10)))
250     // if <4>
251     {
252     ii=i+di;
253     jj=j+dj;
254     ival=*(pixels+NPIXELS*iPos+j*NS+i);
255     if (ival>127)
256     {
257     ival=0;
258     }
259     else
260     {
261     ival=255;
262     }
263     if (((ii>=0) && (ii<NS)) && ((jj>=0) && (jj<NL)))
264     {
265     *(pixies+jj*NS+ii+NPIXELS*0)=(unsigned char) ival;
266     *(pixies+jj*NS+ii+NPIXELS*1)=(unsigned char) ival;
267     *(pixies+jj*NS+ii+NPIXELS*2)=(unsigned char) ival;
268     }
269     } // endif <4>
270     } // endfor <4>
271     } // endfor <3>
272     } // emdif <3>
273     } // endif <2>
274     } // endif <1>
275     } // endfor <2>
276     } // endfor <1>
277     if (flash_count>0)
278     {

```

```

279         return 1;
280     }
281     else
282     {
283         return 0;
284     }
285 }
286
287 int main(void)
288 {
289     int NS; // No. of samples
290     int NL; // No. of lines
291     int NS3; // No. of samples *3
292     int flash_count;
293     int i,j,jj,k,kk;
294     int ip1, ip2, ip3;
295     int flag;
296     int ipos;
297     int ic;
298     int ice;
299     int icount;
300     int nframes; // The No. of TV frames to read in
301     long int NPIXELS;
302     long int NPIXELS3;
303     long int NIMAGES;
304     long int count;
305     FILE *fp;
306     FILE *outy;
307     char fname[12];
308     unsigned char *pixels;
309     unsigned char *pixies;
310     unsigned char *bmp;
311     unsigned char *header; // BMP header for input
312     unsigned char *fheader; // BMP header for output
313     unsigned char *pix;
314     double *avg;
315     double *sd;
316     double sdy;
317
318     printf("What format: 0=NTSC (720x480), 1=NTSC (540x480), 2=PAL (768x576):");
319     scanf("%d",&i);
320     // default NS=720 and NL=480
321     NS=720;
322     NL=480;
323     header=(unsigned char *) malloc(54*sizeof(unsigned char));
324     fheader=(unsigned char *) malloc(54*sizeof(unsigned char));
325
326     if (i==0) // NTSC 720x480
327     {
328         NS=720;
329         NL=480;
330         fp=fopen("ntsc1.dat","rb");
331     }
332     if (i==1) // PAL 640x480
333     {
334         NS=720;
335         NL=480;
336         fp=fopen("ntsc2.dat","rb");
337     }
338     if (i==2) // PAL 768x576

```

```

339 {
340     NS=768;
341     NL=576;
342     fp=fopen("pal.dat","rb");
343 }
344 fread(header,sizeof(unsigned char),54,fp);
345 fclose(fp);
346
347 NPIXELS=NS*NL;
348 NS3=NS*3;
349 NPIXELS3=NPIXELS*3;
350 NIMAGES=60;
351 pixels=(unsigned char *) malloc(NIMAGES*NPIXELS*sizeof(unsigned char));
352 pixies=(unsigned char *) malloc(NPIXELS3*sizeof(unsigned char));
353 bmp=(unsigned char *) malloc(NPIXELS3*sizeof(unsigned char));
354 avg=(double *) malloc(NIMAGES*NPIXELS*sizeof(double));
355 sd=(double *) malloc(NIMAGES*NPIXELS*sizeof(double));
356
357 nframes=0;
358 while (nframes<60)
359 {
360     printf("How many frames to read in?");
361     scanf("%d",&nframes);
362     if (nframes<60) printf("N.B. No. of frames must be >=60\n");
363 }
364
365 /* Initial load up of images */
366 for(i=0;i<60;i++)
367 {
368     sprintf(fname,"a%5d.png",i);
369     for (j=0;j<6;j++)
370     {
371         if (fname[j]==')') fname[j]='0';
372     }
373     fp=fopen(fname,"rb");
374     fread(header,sizeof(unsigned char),54,fp);
375     fread(pixels+NPIXELS*i,sizeof(unsigned char), NPIXELS , fp);
376     fclose(fp);
377 }
378
379
380 /* This computes the sum for the average and the s.d. */
381 sum_average(pixels,NPIXELS,avg);
382 sum_sd(pixels,NPIXELS,avg,sd);
383
384
385
386 ipos=0;
387 icanth=30;
388 ic=30;
389 while (icanth<nframes)
390 {
391     printf("Processing frame %d out of %d\n",icanth,nframes);
392     flash_count=0; // initialize the count of flashes per frame
393
394     if ((icanth%100)==0) // Recompute the average and sd
395     {
396         // This avoids non-systematic rounding errors building up
397         sum_average(pixels,NPIXELS,avg);
398         sum_sd(pixels,NPIXELS,avg,sd);

```

```

399     }
400
401 // Remove the old image from the average sum
402 for (i=0;i<NPIXELS;i++)
403 {
404     sdy=(*pixels+NPIXELS*ic+i))-avg[i]/60.0;
405     sd[i]=sd[i]-sdy*sdy;
406 }
407 for (i=0;i<NPIXELS;i++) avg[i]=avg[i]-(*pixels+NPIXELS*ic+i));
408 // Read in the new image
409 sprintf(fname,"a%5d.png",icount);
410 for (j=0;j<6;j++)
411 {
412     if (fname[j]==',') fname[j]='0';
413 }
414 fp=fopen(fname,"rb");
415 fread(header,sizeof(unsigned char),54,fp);
416 fread(pixels+NPIXELS*ic,sizeof(unsigned char), NPIXELS , fp);
417 fclose(fp);
418
419 // Add the new image back into the average sum
420 for (i=0;i<NPIXELS;i++) avg[i]=avg[i]+(*pixels+NPIXELS*ic+i));
421 for (i=0;i<NPIXELS;i++)
422 {
423     sdy=(*pixels+NPIXELS*ic+i))-avg[i]/60.0;
424     sd[i]=sd[i]+sdy*sdy;
425 }
426
427 if (flash_detector(pixels,pixies,NPIXELS,iPos,NS,NL,avg, sd,&flash_count))
428 {
429     if ((flash_count >= MIN_FLASH_LIMIT) && (flash_count <= MAX_FLASH_LIMIT))
430     {
431         ice=icount-30;
432         sprintf(fname,"b%5d.png",ice);
433         for (j=0;j<6;j++)
434             {
435                 if (fname[j]==',') fname[j]='0';
436             }
437         outy=fopen(fname,"wb");
438         ip1=iPos-1;
439         if (ip1<0) ip1=59;
440         ip2=iPos;
441         ip3=iPos+1;
442         if (ip3>59) ip3=0;
443         fwrite(header,sizeof(unsigned char),54,outy);
444         for (j=0;j<NL;j++)
445             {
446                 jj=NL-1-j;
447                 for (i=0;i<NS;i++)
448                     {
449                         bmp[i*3+0+jj*NS3]=pixies[i+j*NS+0*NPIXELS];
450                         bmp[i*3+1+jj*NS3]=pixies[i+j*NS+1*NPIXELS];
451                         bmp[i*3+2+jj*NS3]=pixies[i+j*NS+2*NPIXELS];
452                     }
453             }
454         fwrite(bmp,sizeof(unsigned char),NPIXELS3,outy);
455         fclose(outy);
456         printf("Video Frame= %d out of %d may have an impact flash %d\n",
457               icount,nframes,ice);
458     }

```

```
459     }
460
461     ipos=ipos+1;
462     ican=ican+1;
463     ic=ic+1;
464     if (ipos>=60) ipos=0;
465     if (ic>=60) ic=0;
466 } // endwhile
467
468 free(sd);
469 free(avg);
470 free(header);
471 free(pixels);
472 free(pixies);
473
474 }
```

Appendix X3

Lunar Impact Flash 1 Region

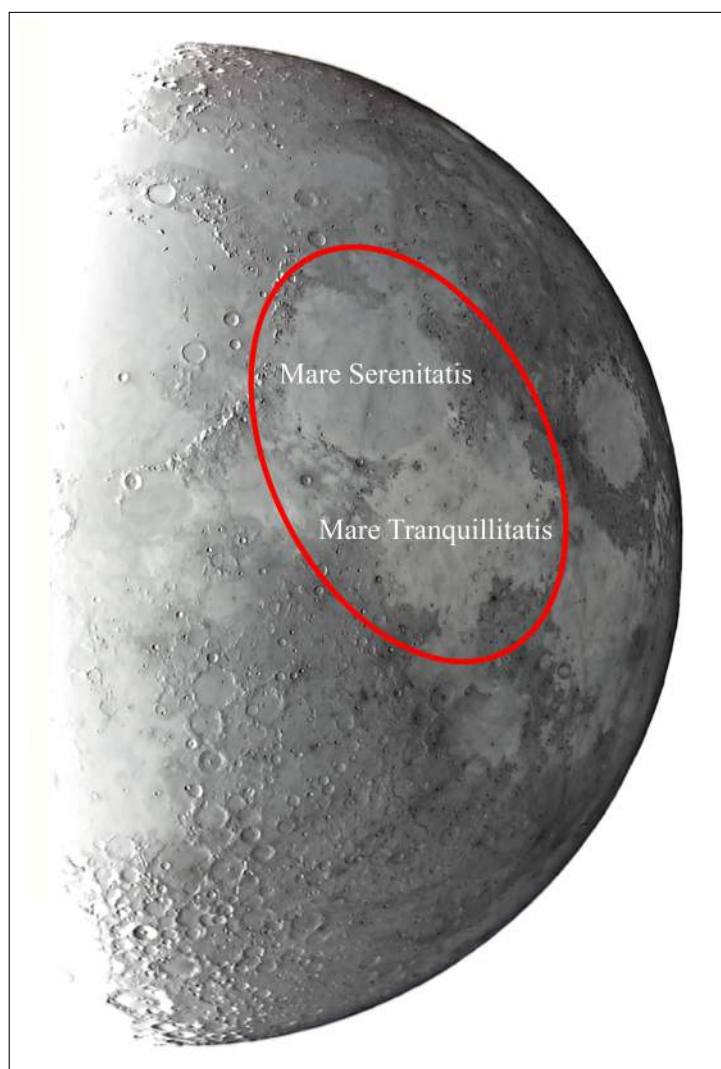


Figure 5: LIF 18/11/2001 231915 UTC ± 12 min. Region circled in red.

Map of the Moon

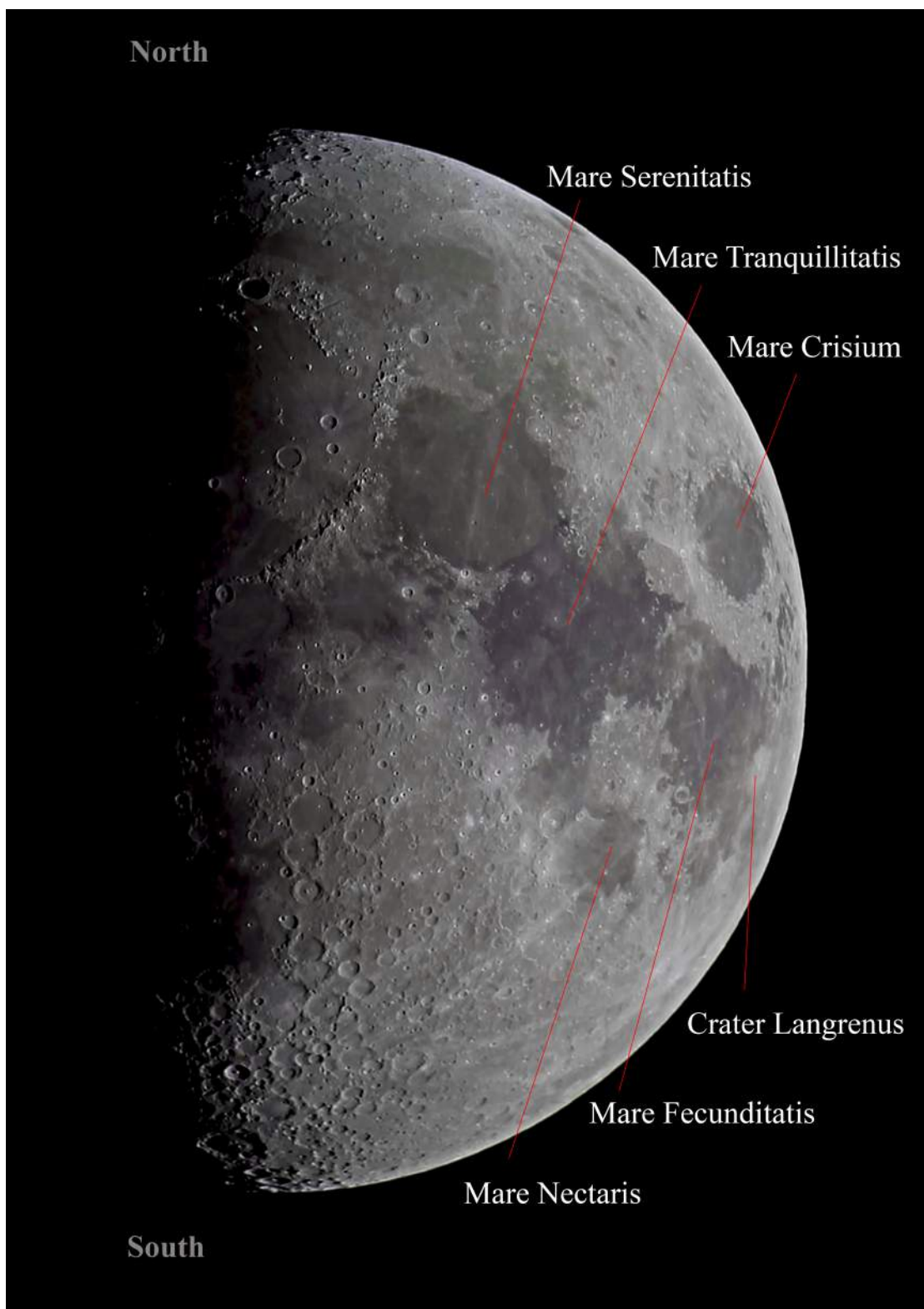


Figure 6: 19/04/2013 2050 UTC ± 12 min. Map of the Moon at 63 % illumination.

Appendix X4

Meteoroid Impact Flash Diagram

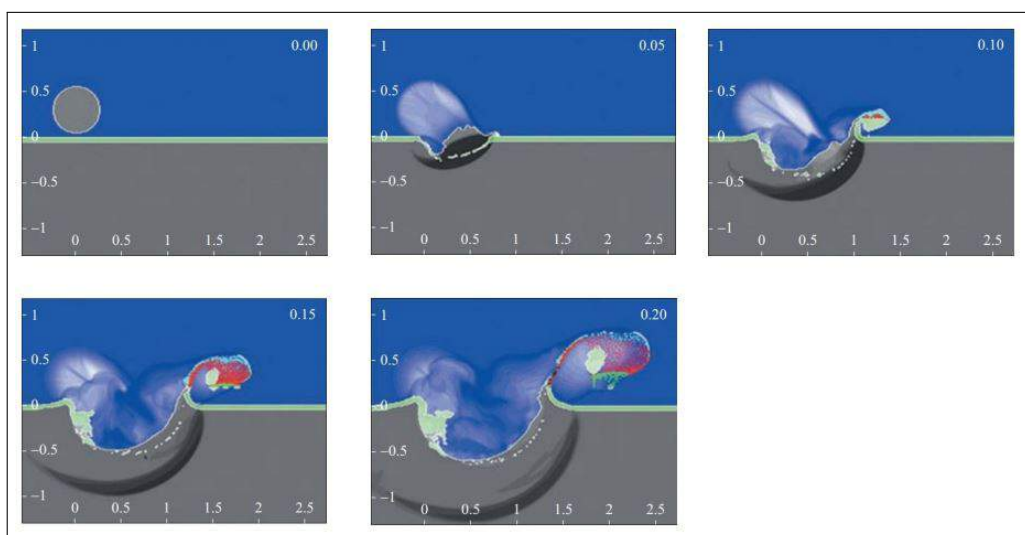


Figure 7: A diagram of a meteoroid impacting the ground and forming a crater. In addition the diagram is used to show the process of an impact flash, with white depicting gas clouds and red representing ejecta melt. Image courtesy of Rothery et al. (2011b).

Index

A

Alt-Azimuth Mount, 13
Audio Video Interleave, 6
Auto-Star Alignment, 12

B

Background Radiation, 21
Bias Frame, 14, 15
Black Body Continuum, 6

C

Cosmic Ray Samples, 23
Cosmic Rays, 8

D

Dark Side, 4
Drop Frames, 6

E

Earth-Shine, 4
Error, 18
European Space Agency, 4
Exosphere, 7
Exposure, 20, 30

F

Field of View, 6, 12
Flux Density, 18
Focal Reducer, 6
Frame Rate, 20
Frames Per Second FPS, 20

G

German Equatorial Mount, 12

H

Helion Meteoroids, 4
Hyper-Velocity Impactors, 1

I

Impact Flash Candidates, 2
Impact Flash Scanner, 15, 33
Infra-Red, 5, 31
Integration Time, 20

K

Kinetic Energy, 5, 6

L

L Shape, 28
LADEE, 4
Leonid's, 4
Luminosity, 18
Luminosity Efficiency, 6
Luminous Efficiency, 5, 30, 37
Luminous Energy, 30, 37
Lunar Phase, 4
LunarScan, 33

M

Magnitude, 6, 8
Mass, 37
Meridian, 12
Meteorite, 4
Meteoroids, 4
Meteors, 4
MinGW, 15
MPEG Streamclip, 15

N

Night Side, 4, 8

O

Optical Wavelength, 31

P

Photomultiplier Tubes, 7
Photons, 14
Pier, 12

Possible Observation, 18

R

Registax , 15

Relative Magnitude, 19

S

Scintillation, 9

SMART-1, 4

Soda-Lime Glass, 7

Solar System, 6

Sun Grazing, 4

T

Terminator Line, 7

Transient Lunar Phenomenon, 4, 8

U

Uncertainties, 18

V

Virtual Dub, 14, 15

W

Waning Crescent, 5

Waning Gibbous, 5

Wavebands, 7

Waxing Crescent, 5

Waxing Gibbous, 5

Z

Zenith, 43

